

# Boosting X-formers with Structured Matrix for Long Sequence Time Series Forecasting

Zhicheng Zhang<sup>a</sup>, Yong Wang<sup>a,\*</sup>, Shaoqi Tan<sup>a</sup>, Bowei Xia<sup>a</sup>, Yujie Luo<sup>a</sup>

<sup>a</sup>*Laboratory of Intelligent Collaborative Computing Technology, University of Electronic Science and Technology of China, Chengdu, 611731, Sichuan, China*

---

## Abstract

Transformer-based models for long sequence time series forecasting problems have gained significant attention due to their exceptional forecasting precision. However, the self-attention mechanism introduces challenges in terms of computational efficiency due to its quadratic time complexity. To address these issues, we propose a novel architectural framework that enhances Transformer models through the integration of Surrogate Attention Blocks (SAB) and Surrogate Feed-Forward Neural Network Blocks (SFB). They replace the self-attention and feed-forward layer by leveraging structured matrices that reduce both time and space complexity while maintaining the expressive power of the original self-attention mechanism and feed-forward network. The equivalence of this substitution is fully demonstrated. Extensive experiments on nine Transformer variants across five distinct time series tasks demonstrate an average performance improvement of 9.45%, alongside a 46% reduction in model size. These results confirm the efficacy of our surrogate-based approach in maintaining prediction accuracy while significantly boosting computational efficiency<sup>1</sup>.

*Keywords:* Long sequence time series forecasting, Self-attention mechanism, Transformer, Structured matrix.

---

## 1. Introduction

Data such as electricity consumption, weather patterns, and traffic flow are collected in the real world using sensors and are referred to as time series data due to their temporal nature. Accurately analyzing and predicting these temporal variations is critical for decision-making in numerous fields such as energy management, transportation optimization, and climate modeling. To achieve this, time series forecasting methods are employed to predict the  $l$ -step future values  $\hat{Y}$  in proximity to the ground truth  $Y = \{y_{N+1}, \dots, y_{N+l}\}$  by utilizing the input sequence  $Z = \{z_1, \dots, z_N\}$ . In particular, it is referred to as a long sequence time

---

<sup>1</sup>Our code is publicly available at <https://github.com/newbeezzc/MonarchAttn>

\*Corresponding author

*Email address:* [cla@uestc.edu.cn](mailto:cla@uestc.edu.cn) (Yong Wang)

series forecasting (LSTF) task when both  $l$  and  $N$  are large, which is often the case in high-frequency measurement systems generating vast amounts of data. Over the past few years, a variety of Transformer-based neural network models (a.k.a. *X-formers*) have demonstrated their remarkable success in the LSTF task.

These *X-formers* rely on the self-attention mechanism to capture trend, seasonal, and remainder patterns within a time series by linking all tokens in the sequence through relevance-based scoring functions. It is particularly beneficial in measurement science, where understanding the interrelationships between different measurement points can lead to more accurate predictions and better insights into the observed phenomena. However, the self-attention mechanism has a quadratic time and memory complexity with respect to  $N$ , making *X-formers* computationally demanding and challenging to use in LSTF tasks under limited resources.

From the perspective of time series sequence features, the attention mechanism is able to capture the latent dependencies between arbitrary data points in the time series sequence. Unfortunately, due to the absence of inductive biases, it lacks the ability to capture temporal causality and trend features, which slows down their convergence during the training phase. Consequently, a large amount of data samples are required to train a Transformer-based model so that it can achieve satisfactory forecasting results. Current *X-formers* are rooted in the observation of the scoring matrix in the self-attention mechanism, which exhibits two key properties: locality [1] and sparsity [2].

The locality property suggests that tokens primarily interact with their neighbors. With such observation, the works in [3, 4] theoretically proved that multi-head self-attention and convolution are similar in expressiveness, which suggests that it can obtain better efficiency by using convolutional layers to replace self-attention layers. Similarly, other works[5, 6] further integrated convolutional operations into self-attention layers guided by this property, which led to reduced model complexity and better prediction accuracy. The sparsity arises from the fact that most elements in the attention score matrix are close to zero, indicating that only a few tokens are crucial for LSTF tasks. Exploiting this sparsity, researchers in [7, 8, 9] have employed techniques such as down-sampling and memory compression to alleviate the time and memory complexity of *X-formers*. These two properties offer valuable insights into optimizing Transformer-based models for LSTF, ultimately leading to improved performance and efficiency. Current works focus on the model-level design, apparently ignoring the success of previous Transformer-based models in the LSTF task.

Another branch of work attempts to create a lightweight model through parameter quantification[10, 11, 12], LSTF-specific knowledge distillation[13, 14] and network pruning[15, 16]. These works are model and task specific because they assume the existence of a well-trained Transformer. Furthermore, they have to strike a balance between efficiency, accuracy, and expressiveness.

In order to inherit the successful experience of the existing *X-formers* and improve the efficiency of *X-formers* without compromising their performance, the following questions need to be addressed: (1) Is there an efficient computational method that is sub-quadratic in both sequence length and model dimension? (2) Based on such a method, is it possible to develop independent modules that can replace the cumbersome layers in the existing *X-*

*formers* without altering their architecture? (3) Does the replacement method possess the equivalent expressive power as the *X-formers*?

In addressing these questions, we have condensed our research into three main aspects:

- Through structural-level analysis of the *X-formers*, the self-attention and feed-forward neural network layers are targeted as having the highest computational overhead in these models. The Surrogate Attention Block (SAB) and Surrogate FFN Block (SFB) are designed to replace them (denoted as *X-formers*<sup>\*</sup>), reducing both computational and space complexity while maintaining the predictive accuracy of the model itself.
- The equivalence between *X-former*<sup>\*</sup> and *X-former* is established from the perspective of the two surrogate blocks. We further show that the SAB block has a similar ability to capture both long- and short-term dependencies of the time series sequences.
- The comparative experiments were performed on 9 *X-formers* for 5 types of time series tasks. The experimental results show that *X-formers*<sup>\*</sup> outperform the corresponding *X-formers* in 60.8% of the total 2349 tasks. The average improvement is 9.45%, with a 6.35% reduction in computation time and a 46% reduction in model size.

The rest of the article is organized as follows: The related works are reviewed in Section 2. Section 3 reviews the prior knowledge needed for the article. Section 4 describes the two surrogate blocks and proves the equivalence of the attention layer and the convolution. Section 5 contains a proof of the expressive power of the substitution module, an analysis of the complexity and a proof of stability. The experimental evaluations are presented in Section 6. Finally, some brief discussion and conclusions are drawn in Section 7.

## 2. Related works

The works in [17, 18, 8, 19, 20, 21] introduce enriched positional embedding mechanisms to guide the self-attention in capturing both local patterns and long-range dependencies in the time series sequences. These variants showed their adaptability in handling complex real-world LSTF application scenarios.

Other studies[6, 22] hybridize various neural network components, such as convolution[23, 9] and LSTM[24], with attention mechanisms to achieve higher model capacity and better generalization. However, these module-level or architecture-level modifications of Transformers focus on accommodating a specific challenge in LSTF, which results in increased complexity and subsequent sluggishness of their models.

The computational complexity and memory bottleneck of the self-attention mechanism in *X-formers* have been thoroughly analyzed. To enhance efficiency, some research, such as LogTrans[9] and Informer[8], focuses on exploiting the inherent sparsity and locality in the attention score matrix. They employ approximation calculations by down-sampling in self-attention layers, reducing computational complexity to  $O(N \log N)$ . TCCT[25], GCformer[26], Autoformer[6], and MODERNNTCN[27] propose replacing self-attention layers with convolutional layers due to their equivalence. These approaches are efficient in

Model	Complexity	Task Type	Structured matrix	Series Decomposition	Hardware-friendly	DownSampling
Autoformer[6]	$O(N \log N)$	LSTF	✗	✓	✗	✓
FEDformer[19]	$O(N)$	LSTF	✗	✓	✗	✓
Preformer[38]	$O(\frac{N^2}{L_{seg}})$	LSTF	✗	✓	✗	✗
Informer[8]	$O(N \log N)$	LSTF	✗	✗	✗	✓
NST[39]	$O(N^2)$	LSTF	✗	✗	✗	✗
Pyraformer[22]	$O(N)$	LSTF	✗	✗	✗	✗
Crossformer[40]	$O(\frac{D}{L_{seg}^2} N^2)$	LSTF	✗	✗	✗	✗
ETSformer[28]	$O(N \log N)$	LSTF	✗	✓	✗	✓
FPPformer[41]	$O(NP)$	LSTF	✗	✗	✗	✗
GCformer[26]	$O(N^2)$	LSTF	✗	✓	✗	✗
Conformer[42]	$O(\omega N)$	LSTF	✗	✓	✗	✗
PDFormer[43]	$O(N^2)$	STSF	✗	✗	✗	✗
TFT[18]	$O(N^2)$	MHSF	✗	✗	✗	✗
Yformer[44]	$O(N \log N)$	LSTF	✗	✓	✗	✓
TCCT[25]	$O(\frac{1}{2}N^2)$	LSTF	✗	✗	✗	✓
Quatformer[45]	$O(2cN)$	LSTF	✗	✓	✗	✗
AST[46]	$O(N \log N)$	LSTF	✗	✗	✗	✓
Spacetimeformer[47]	$O(N^2)$	STSF	✗	✗	✗	✗
LogTrans[9]	$O(N \log N)$	LSTF	✗	✗	✗	✓
TDformer[48]	$O(N \log N)$	LSTF	✗	✓	✗	✗
Taylorformer[49]	$O(N^2)$	LSTF	✗	✗	✗	✗
iTransformer[50]	$O(N^2)$	LSTF	✗	✗	✗	✗
Ours	$O(N^{3/2})$	LSTF	✓	✗	✓	✗

Table 1: Comparison of Transformer Variants. P is the patch size. N generally refers to the sequence length. D is the dimension of the data.  $L_{seg}$  represents segment length.  $\omega$  denotes fixed window size. c is a hyperparameter relying on the characteristics of the time series dataset. LSTF, MHSF, and STSF represent Long Sequence Time Series Forecasting, Multi-horizon Forecasting, and Spatio-Temporal Time Series Forecasting, respectively

capturing local dependencies and suitable for training with fewer parameters. Other studies utilize low-rank factorization to enhance efficiency. For instance, FEDformer[19] and ETSformer[28] transform time series into the frequency domain to construct frequency attention using the Fast Fourier Transform (FFT).

Some research[29, 30, 31] suggests using Singular Value Decomposition (SVD), Non-negative Matrix Factorization (NMF)[32, 33] and Sparse Coding[34, 35] to simplify high-dimensional self-attention scoring matrices into lower-dimensional forms. Table 1 compares our method with *X-formers* on various time series tasks in recent years in six dimensions. Our approach achieves a balance between computational complexity and memory usage, with a complexity of  $O(N^{3/2})$  while maintaining structured matrix operations and hardware-friendly characteristics. This allows our method to efficiently handle long sequence time series forecasting tasks, where other *X-formers* may encounter limitations in terms of computational efficiency or memory requirements.

In addition to the previously discussed optimization techniques, there are additional strategies that can be employed to reduce model size and improve computational efficiency. Branching[36, 37] provides advanced architectural optimization, allowing for more efficient network structures. Quantification[10, 11, 12] enables model compression through parameter reduction, significantly reducing computational requirements. The process of knowledge distillation[13, 14] is useful in transferring complex model knowledge to smaller models, improving computational efficiency. Pruning[15, 16] involves removing non-critical neurons or connections to streamline the network to improve computational efficiency.

### 3. Preliminaries

#### 3.1. Revisiting Transformer mechanisms

*X-formers* follow the encoding-decoding structure, which essentially comprises the components of Multi-Head Self-Attention (MHSA) layer, Feed-Forward Network (FFN) layer, and Residual Connections (RC).

An **MHSA layer** utilizes multiple self-attentions as heads to extract different types of features, which is widely used in practice. Let  $z_t \in \mathbb{R}^m$  denote the observation of  $m$  variables at time step  $t$ . Given a multivariate time series sequence  $\mathbf{Z} = \{z_1, z_2, \dots, z_N\} \in \mathbb{R}^{N \times m}$  for  $N$  time steps,  $\mathbf{Z}$  can be projected as the representation  $\mathbf{X} \in \mathbb{R}^{N \times D_{in}}$ . For the input representation  $\mathbf{X}$ , self-attention matches the sequence of queries  $Q = \mathbf{X}W_{qry} \in \mathbb{R}^{N \times D_k}$  against the sequence of keys  $K = \mathbf{X}W_{key} \in \mathbb{R}^{N \times D_k}$  by scaled dot-product. The output of an MHSA layer can be formulated as:<sup>2</sup>

$$SA^{(h)}(\mathbf{X}) := \text{Softmax} \left( \frac{Q^{(h)} \cdot (K^{(h)})^T}{\sqrt{D_k}} \right) \cdot \mathbf{X} \cdot W_{val}^{(h)}$$

$$MHSA(\mathbf{X}) := \text{concat}_{h \in [H]}[SA^{(h)}(\mathbf{X})] \cdot W_{out}$$

where  $W_{val}^{(h)} \in \mathbb{R}^{D_{in} \times D_v}$  and  $W_{out} \in \mathbb{R}^{(HD_v) \times D_{out}}$  are learnable projection matrices.  $H$  is the number of heads.

An **FFN layer** typically consists of two-layer neural networks, which can be expressed as:

$$FFN(\mathbf{X}) = \sigma(\mathbf{X} \cdot W_1) \cdot W_2^T$$

where  $W_1, W_2 \in \mathbb{R}^{D_{in} \times D_m}$  are learnable parameter matrices,  $\sigma$  is a non-linearity function such as *ReLU*.

An **RC** connects the inputs and outputs of a sub-layer in transformers such as FFN and MHSA. Considering the position of the normalization layer in transformers, there are currently two major definitions of residual connections, which are:

$$\mathbf{X} = LN(\mathbf{X} + F(\mathbf{X}))$$

and

$$\mathbf{X} = \mathbf{X} + F(LN(\mathbf{X}))$$

where  $LN(\cdot)$  is the layer normalization function,  $F(\cdot)$  is a sub-layer (e.g., FFN or MHSA).

#### 3.2. Structured matrices

Structured matrices are those with a sub-quadratic number of parameters and runtime. Large classes of structured matrices (e.g., Toeplitz-like[51], ACDC[52], Fastfood[53], and Butterfly[54]) have demonstrated their capacities of replacing dense weight matrices in large

---

<sup>2</sup>For easy-to-understand presentation, biases are excluded in the following equations.

neural networks, which can reduce their computation and memory requirements. Very recently, Monarch matrices were proposed to capture a wide class of linear transforms, including Hadamard transforms, Toeplitz matrices, ACDC matrices, and convolutions. They are a sub-quadratic class of structured matrices that are hardware-efficient and expressive [55]. A Monarch matrix  $\mathbf{M} \in \mathbb{R}^{N \times N}$  of order- $p$  is defined as:

$$\mathbf{M} = \left( \prod_{i=1}^p \mathbf{P}_i \mathbf{B}_i \right) \mathbf{P}_0$$

where each  $\mathbf{P}_i$  is associated with the ‘base  $\sqrt[p]{N}$ ’ variant of the bit-reversal permutation, and  $\mathbf{B}_i$  is a block-diagonal matrix with a block size of  $b$ . When setting  $p = 2$  and  $b = \sqrt{N}$ , Monarch matrices require  $O(N^{3/2})$  computed in a time series sequence of length  $N$ .

### 3.3. Acceleration objectives

Compute-bound and memory-bound [56] are two classes of operations on GPUs that mainly affect the runtime performance of deep learning models. The FLOP/s is used as a metric to determine the speed of these operations. Therefore, the objectives of accelerating long sequence time series forecasting models are sub-quadratic scaling with the input length  $N$  and high FLOP utilization. Let  $O_{\text{computation}}(\cdot)$  and  $O_{\text{memory}}(\cdot)$  be the computation and memory complexity of a model. For a given well-designed  $X$ -former, it is accelerated or enhanced as  $X$ -former $^*$  that satisfies:

$$\begin{aligned} O_{\text{computation}}(X\text{-former}^*(X)) &< O_{\text{computation}}(X\text{-former}(X)) \\ O_{\text{memory}}(X\text{-former}^*(X)) &< O_{\text{memory}}(X\text{-former}(X)) \end{aligned}$$

Subject to:

$$E_{\hat{Y}}(\|X\text{-former}^*(\mathbf{X}) - X\text{-former}(\mathbf{X})\|) < \varepsilon$$

where  $E(\|\cdot\|)$  is an evaluation function that measures the accuracy of  $h$  steps time series forecasting results on labeled sequences  $\hat{Y} = \{\hat{y}_{N+1}, \hat{y}_{N+2}, \dots, \hat{y}_{N+h}\}$ , such as Mean Square Error (MSE).  $\varepsilon$  indicates the difference between the output of  $X$ -former $^*$  and  $X$ -former. Ideally, we suppose  $\varepsilon$  can be ‘ignored’. The major notations used in this article are presented in Table 2.

## 4. Methodology

Given any  $X$ -former, structured matrices are used in X-MHSA and FFN layers to substitute the matrix calculations in the linear transformations (denoted as Surrogate Attention Block and Surrogate FFN Block), thereby reducing the computational cost while preserving the characteristics of the  $X$ -former architecture. Figure 1 demonstrates our substitution framework, vividly illustrating how the substitution framework improves computational efficiency by replacing key computational steps.

Notations	Descriptions
$\mathbf{Z}$	Input time series
$\mathbf{Y}$	Ground truth future time series for forecasting
$\hat{\mathbf{Y}}$	Predicted future time series
$\mathbf{X}$	Embedding in model
$W$	Weight matrix
$\mathbf{M}$	Structured matrix
$Q, K, V$	Query, key and value matrix in attention layers
$N$	Length of the input time series
$m$	Dimension of the input time series
$l$	Length of prediction
$D_{in}$	Dimension of a layer input
$D_{out}$	Dimension of a layer output
$D_k$	Dimension of queries and keys
$D_v$	Dimension of values
$H$	Number of heads
$h$	Index of head
$p$	Order of Monarch matrix
$q$	Index of time step in queries
$k$	Index of time step in keys

Table 2: Notations and Descriptions

#### 4.1. Surrogate Attention Block

The Surrogate Attention Block consists of two main steps: linear projection substitution and attention substitution.

##### 4.1.1. Linear Projection Substitution

Monarch matrices have been demonstrated to capture Hadamard transforms, specifically matrix multiplication [57]:

**Remark 1.** Let  $H_n$  be the Hadamard Transform of size  $n$ . Then,  $H_n \in \mathcal{M}$ .

**Proposition 1.** Let  $W$  be a weight matrix; a linear projection  $\text{LinearProj}(\mathbf{X}) = \mathbf{X}W$  is equivalent to a structured linear projection  $\text{StructuredLinearProj}(\mathbf{X}) = \mathbf{X}\mathbf{M}$ , where  $\mathbf{M}$  is a structured matrix.

**Proof 1.** Proof follows from Remark 1.

In accordance with Proposition 1, the linear projection in MHSA can be reformulated as:

$$Q^{(h)} = \mathbf{X}\mathbf{M}^{1(h)}, \quad K^{(h)} = \mathbf{X}\mathbf{M}^{2(h)}, \quad V^{(h)} = \mathbf{X}\mathbf{M}^{3(h)} \quad (1)$$

where  $\mathbf{M}^{*(h)}$  denotes the Structured matrix on  $h$ -th head.

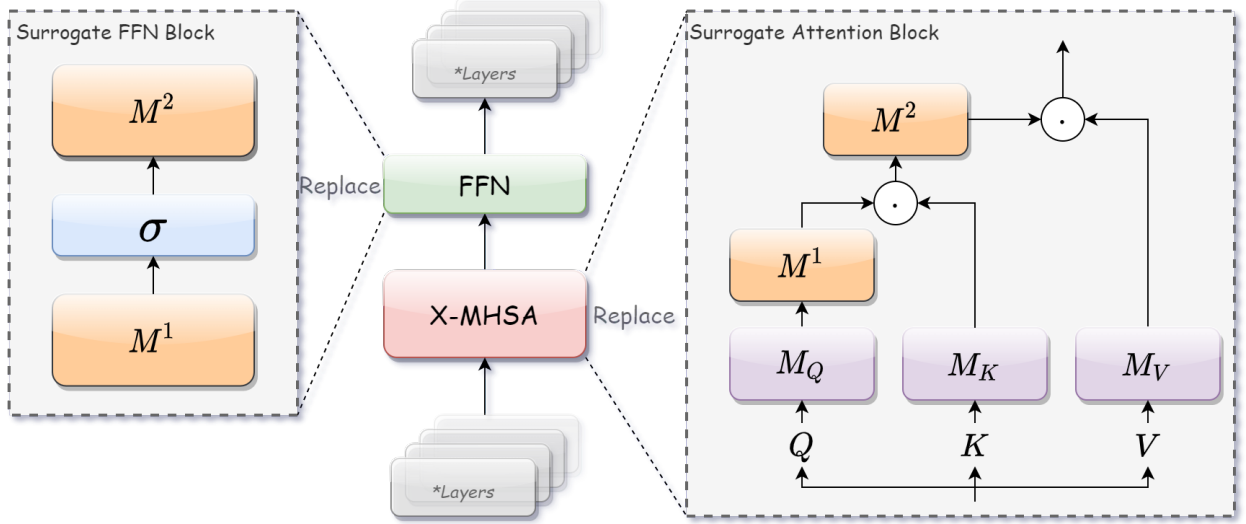


Figure 1: Overview of the proposed enhancement process for an *X-former*. For ease of presentation, here only one XMHSA layer and one FNN layer are illustrated in the *X-former*, neglecting the encoder-decoder architecture, multi-layer stacking, and other layers that were not modified.

#### 4.1.2. Attention Substitution

In order to reduce the computational consumption in the attention mechanism, take inspiration from articles utilizing gated long convolution to replace the attention mechanism [58, 59, 60, 55]. Based on the FFT convolution theorem<sup>3</sup>, we propose substituting XMHSA with:

$$\begin{aligned} SA^{(h)}(\mathbf{X}) &:= \mathbf{M}^2 (\mathbf{M}^1 Q^{(h)} \odot K^{(h)}) \odot V^{(h)} \\ MHSA(\mathbf{X}) &:= \sum_{h \in [H]} SA^{(h)}(\mathbf{X}) W_{out}^{(h)} \end{aligned} \quad (2)$$

where  $\mathbf{M}^1, \mathbf{M}^2 \in \mathbb{R}^{N \times N}$  are Structured matrices represent *FFT* and *FFT*<sup>-1</sup>,  $\odot$  denotes element-wise multiplication, and  $W_{out}^{(h)}$  denotes the output projection matrix. Here, the key matrix  $K$  is treated as the convolutional kernel.

Since the attention mechanism and convolution are not exactly equivalent, to demonstrate the validity of this substitution, the question must be answered: *under what conditions can an MHSA layer be replaced by a (several) convolutional layer(s) in time series tasks?*

Under observations of patterns in the self-attention score matrix of LSTF, they can be categorized into four distinct types[61]: diagonal, vertical, block and heterogeneous.

Within the context of the diagonal pattern, self-attention aggregates local information for each query to capture seasonal patterns within the region centered on itself, reflecting element-level local dependencies. When all heads in an MHSA layer exhibit a diagonal pattern, it is termed a diagonal MHSA layer. On the  $h$ -th head of a diagonal MHSA layer,

<sup>3</sup> $\mathbf{K} * \mathbf{X} = FFT^{-1} (FFT(\mathbf{X}) * FFT(\mathbf{K}))$

the score matrices can be expressed as:

$$A_{q,k}^{(h)} = \begin{cases} f^{(q,h)}(q-k) & (q-k) \in \Delta \\ 0 & \text{otherwise} \end{cases} \quad (3)$$

where  $A_{q,k}^{(h)}$  denotes the element at position  $(q, k)$  in the score matrix,  $\Delta = \{-\lfloor \lambda/2 \rfloor, \dots, \lfloor \lambda/2 \rfloor\}$  contains all the corresponding shifts in the diagonal local region with size  $\lambda$ , and  $f^{(q,h)}$  is a set of functions:  $f^{(q,h)} : \Delta \rightarrow (0, 1]$ . For fixed  $q$  and  $h$ ,  $\sum_{\delta \in \Delta} f^{(q,h)}(\delta) = 1$ .

**Theorem 1.** Suppose  $\exists h \in [H], \forall q_1, q_2 \in [N], f^{(q_1,h)} = f^{(q_2,h)}$ , a diagonal MHSA layer with the diagonal local region size  $\lambda$ , the heads number  $H$ , the head dimension  $D$  and output dimension  $D_{out}$  is equivalent to a **sum of convolutional layer** of kernel size  $\lambda$  and  $D_{out}$  output channels, i.e.,  $MHSA^D(\mathbf{X}) = \sum_{h \in [H]} Conv^{(h)}(\mathbf{X})$ .

Under the vertical pattern, self-attention maps the specific local regions to each query to learn the relationships between different local regions, which reflect the region-level local dependencies. When all heads in an MHSA layer exhibit a distinct vertical pattern, it is termed a vertical MHSA layer. On the  $h$ -th head of a vertical MHSA layer, the score matrices can be expressed as:

$$A_{q,k}^{(h)} = \begin{cases} g^{(q,h)}(k) & k \in \tilde{K}^{(h)} \\ 0 & \text{otherwise} \end{cases} \quad (4)$$

where  $A_{q,k}^{(h)}$  denotes the element at position  $(q, k)$  in the score matrix,  $\tilde{K}^{(h)} = \{\tilde{k}_1^{(h)}, \dots, \tilde{k}_{\lambda}^{(h)}\}$  contains all  $\lambda$  significant columns, and  $g^{(q,h)}$  is a set of functions:  $g^{(q,h)} : \tilde{K}^{(h)} \rightarrow (0, 1]$ . For fixed  $q$  and  $h$ ,  $\sum_{k \in \tilde{K}^{(h)}} g^{(q,h)}(k) = 1$ .

**Theorem 2.** Suppose  $\exists h \in [H], \forall q_1, q_2 \in [N], g^{(q_1,h)} = g^{(q_2,h)}$ , a vertical MHSA layer with the significant columns number  $\lambda$ , the heads number  $H$ , the head dimension  $D$  and output dimension  $D_{out}$  is equivalent to a **sum of convolutional layer** of kernel size  $\lambda$  and  $D_{out}$  output channels, i.e.,  $MHSA^V(\mathbf{X}) = \sum_{h \in [H]} Conv^{(h)}(\mathbf{X})$ .

Theorems 1 and 2 are proved by incorporating Eq. (3) and Eq. (4) into the expression for MHSA (Eq. (1)). By crafting a bijective mapping and leveraging the law of the union of matrix multiplications, each head of a diagonal or vertical MHSA layer can be represented as a convolution expression. Please refer to Appendix A.1 and Appendix A.2 for a comprehensive elucidation of the proof procedure.

Under the block and heterogeneous pattern which appear less frequently in LSTF[61], it can be considered that each block in the attention map is a convolutional kernel (where a heterogeneous pattern is regarded as one block). Since the block size is large, it is challenging to regard this as meeting the requirement of capturing local features in the convolution. However, it aligns with the concept of a long convolution with a massive kernel. Therefore, the block and the heterogeneous MHSA layer can be equivalent to a long convolution. Nevertheless, this equivalence is not strict, as it does not meet the requirement of weight sharing in a long convolution.

#### 4.2. Surrogate FFN Block

The Transformer-based architecture stipulated the inclusion of a feed-forward neural network (FFN) layer following each self-attention layer, a configuration retained by many X-formers. Following Proposition 1, the dense weight matrices can simply swapped out in the FFN block with structured matrices[55]:

$$\mathbf{Y} = \sigma(\mathbf{X}\mathbf{M}^1)\mathbf{M}^2 \quad (5)$$

where  $\sigma$  is an optional point-wise non-linearity (e.g. ReLU),  $\mathbf{M}^1, \mathbf{M}^2 \in \mathbb{R}^{D \times D}$  are Structured matrices. The leftmost side of Figure 1 illustrates the replacement of FFNs.

### 5. Theoretical analysis

#### 5.1. Expressiveness

This section demonstrates the expressiveness of the Surrogate Attention Block on time series tasks by describing its parameterization for solving time series forecasting tasks.

Consider a simple time series with 4 time steps :  $\mathbf{X} = \{x_0, x_1, x_2, x_3\}$ . If this time series exhibits **short-term dependence**, it indicates a strong relationship between the value at one time step and the value at the previous time step. Taking  $x_1$  as an example, its output  $y_1$  must be related to  $x_0$ . Recall Eq.(2) and  $\mathbf{M}^1 = \mathbf{P}\mathbf{L}^1\mathbf{P}\mathbf{R}^1\mathbf{P}$ ,  $\mathbf{M}^2 = \mathbf{P}\mathbf{L}^2\mathbf{P}\mathbf{R}^2\mathbf{P}$ , the following exist:

$$y_1 = v_1(\mathbf{L}_{2,2}^2 (\mathbf{R}_{1,0}^2 a_0 + \mathbf{R}_{1,1}^2 a_2) + \mathbf{L}_{2,3}^2 (\mathbf{R}_{3,2}^2 a_1 + \mathbf{R}_{3,3}^2 a_3))$$

where the subscripts denote the elements in the corresponding positions in the matrix, and

$$\begin{aligned} a_0 &= k_0(\mathbf{L}_{0,0}^1 (\mathbf{R}_{0,0}^1 q_0 + \mathbf{R}_{0,1}^1 q_2) + \mathbf{L}_{0,1}^1 (\mathbf{R}_{2,2}^1 q_1 + \mathbf{R}_{2,3}^1 q_3)) \\ a_1 &= k_1(\mathbf{L}_{2,2}^1 (\mathbf{R}_{1,0}^1 q_0 + \mathbf{R}_{1,1}^1 q_2) + \mathbf{L}_{2,3}^1 (\mathbf{R}_{3,2}^1 q_1 + \mathbf{R}_{3,3}^1 q_3)) \\ a_2 &= k_2(\mathbf{L}_{1,0}^1 (\mathbf{R}_{0,0}^1 q_0 + \mathbf{R}_{0,1}^1 q_2) + \mathbf{L}_{1,1}^1 (\mathbf{R}_{2,2}^1 q_1 + \mathbf{R}_{2,3}^1 q_3)) \\ a_3 &= k_3(\mathbf{L}_{3,2}^1 (\mathbf{R}_{1,0}^1 q_0 + \mathbf{R}_{1,1}^1 q_2) + \mathbf{L}_{3,3}^1 (\mathbf{R}_{3,2}^1 q_1 + \mathbf{R}_{3,3}^1 q_3)) \end{aligned}$$

For simplistic considerations, we ignore projections of queries, keys and values. Let:

$$\mathbf{L}^1 = \begin{bmatrix} 1 & 0 & & \\ 0 & 0 & & \\ & 0 & 0 & \\ & 0 & 0 & \end{bmatrix}, \mathbf{R}^1 = \begin{bmatrix} 1 & 0 & & \\ 0 & 0 & & \\ & 0 & 0 & \\ & 0 & 0 & \end{bmatrix}, \mathbf{L}^2 = \begin{bmatrix} 0 & 0 & & \\ 0 & 0 & & \\ & 1 & 0 & \\ & 0 & 0 & \end{bmatrix}, \mathbf{R}^2 = \begin{bmatrix} 0 & 0 & & \\ 1 & 0 & & \\ & 0 & 0 & \\ & 0 & 0 & \end{bmatrix}$$

it yields  $y_1 = x_0^2 x_1$ , which makes  $y_1$  and  $x_0$  strongly correlated, confirming that Surrogate Attention Block can learn short-term dependencies.

**Long-term dependence** means that  $\mathbf{X}$  will exhibit periodicity. For example, if the period of  $\mathbf{X}$  is assumed to be 2, then  $x_2$  will be strongly correlated with  $x_0$ . Recall Eq.(2) and  $\mathbf{M}^1 = \mathbf{P}\mathbf{L}^1\mathbf{P}\mathbf{R}^1\mathbf{P}$ ,  $\mathbf{M}^2 = \mathbf{P}\mathbf{L}^2\mathbf{P}\mathbf{R}^2\mathbf{P}$ , the following relations exist:

$$y_2 = v_2(\mathbf{L}_{1,0}^2 (\mathbf{R}_{0,0}^2 a_0 + \mathbf{R}_{0,1}^2 a_2) + \mathbf{L}_{1,1}^2 (\mathbf{R}_{2,2}^2 a_1 + \mathbf{R}_{2,3}^2 a_3)) \quad (6)$$

Metric	MSE	MAE
Long	96	0.0046 0.0619
	192	0.0063 0.0723
	336	0.0079 0.0779
	720	0.0107 0.0907
Short	96	0.0094 0.0882
	192	0.0097 0.0901
	336	0.0132 0.1049
	720	0.0106 0.0912

Table 3: The experimental results of validating the replacement method on the artificial datasets.

where  $a_0, a_1, a_2, a_3$  are the same as those shown above.

Also, we ignore projections of queries, keys and values. Let:

$$\mathbf{L}^1 = \begin{bmatrix} 1 & 0 \\ 0 & 0 \\ & 0 & 0 \\ & 0 & 0 \end{bmatrix}, \mathbf{R}^1 = \begin{bmatrix} 1 & 0 \\ 0 & 0 \\ & 0 & 0 \\ & 0 & 0 \end{bmatrix}, \mathbf{L}^2 = \begin{bmatrix} 0 & 0 \\ 1 & 0 \\ & 0 & 0 \\ & 0 & 0 \end{bmatrix}, \mathbf{R}^2 = \begin{bmatrix} 1 & 0 \\ 0 & 0 \\ & 0 & 0 \\ & 0 & 0 \end{bmatrix}$$

it yields that  $y_2 = x_2 x_0^2$ , which makes time step 2 and time step 0 strongly correlated, confirming that Surrogate Attention Block can learn long-term dependencies. We also prove the case with time step  $N$  in Appendix A.4.

In addition, we also attempt to empirically demonstrate that our proposed method can adapt to long-term and short-term time series. A long-term datasets are generated using a sine function with a period of 96 and short-term datasets using a sine function with a period of 7. Subsequently, we conducted experiments on these two artificial datasets using the improved Transformer model (see Table 3). The prediction errors for each task were close to zero, empirically demonstrating that our method effectively captures long-term and short-term dependencies in time series data.

### 5.2. Complexity

Since this paper mainly utilizes the Monarch matrix, here we first show that an order-2 Monarch matrix  $\mathbf{M} = \mathbf{P} \mathbf{L} \mathbf{P}^T \mathbf{R} \mathbf{P} \in \mathbb{R}^{n \times n}$  is described by  $2n^{3/2}$  parameters: both  $\mathbf{L}, \mathbf{R}$  have  $n^{1/2}$  dense blocks of size  $n^{1/2} \times n^{1/2}$ , each with a total number of parameters of  $n^{3/2}$ . The permutation  $\mathbf{P}$  is fixed, so no parameters are added. In order to multiply by  $\mathbf{M}$ , permute, multiply by the block diagonal matrix  $\mathbf{R}$ , permute, multiply by the block diagonal matrix  $\mathbf{L}$ , and finally permute are needed (when right-multiplying by  $\mathbf{M}$ , this order is reversed). When these five steps are effectively executed, the total time complexity is  $O(n^{3/2})$ .

Table 4 shows the summary of complexity variations. Our proposed replacement method will decrease the time complexity from  $O(N^2D + ND^2)$  to  $O(N^{3/2}D + ND^{3/2})$  and the space complexity from  $O(D^2)$  to  $O(D^{3/2} + N^{3/2})$ . The following subsections provide detailed explanations of the complexity changes in three neural networks.

Layer	Time Complex	Space Complex
LP	$O(ND^2) \rightarrow O(ND^{\frac{3}{2}})$	$O(D^2) \rightarrow O(D^{\frac{3}{2}})$
Attention	$O(N^2D) \rightarrow O(N^{\frac{3}{2}}D)$	$0 \rightarrow O(N^{\frac{3}{2}})$
FFN	$O(ND^2) \rightarrow O(ND^{\frac{3}{2}})$	$O(D^2) \rightarrow O(D^{\frac{3}{2}})$
Total	$O(N^2D + ND^2) \rightarrow O(N^{\frac{3}{2}}D + ND^{\frac{3}{2}})$	$O(D^2) \rightarrow O(D^{\frac{3}{2}} + N^{\frac{3}{2}})$

Table 4: Summary of complexity variations.

### 5.2.1. Linear Projection (LP)

In a linear projection layer, the input is multiplied by a weight matrix, its time complexity is  $O(ND^2)$ , space complexity is only related to the size of the weight matrix, i.e.  $O(D^2)$ . After substituting the weight matrix by Monarch matrix, the time complexity of linear projection is reduced to  $O(ND^{3/2})$  and the space complexity is reduced to  $O(D^{3/2})$ .

### 5.2.2. Attention

The attention layer consists of three steps: (1) **Score matrix calculation**: Multiplication of matrices of size  $N \times D$  and  $D \times N$ , with a complexity of  $O(N^2D)$ . (2) **Softmax**: Softmax calculation for each row of the score matrix, with a complexity of  $O(N)$  for one softmax calculation, thus the complexity for  $N$  rows is  $O(N^2)$ . (3) **Weighted sum**: Multiplication of matrices of size  $N \times D$  and  $D \times N$ , with a complexity of  $O(N^2D)$ . In total, the time complexity is  $O(N^2D) + O(N^2) + O(N^2D) = O(N^2D)$ . The surrogate attention block includes two matrix dot products and two Monarch matrix multiplications, with a total time complexity of  $2 \times O(ND) + 2 \times O(N^{3/2}D) = O(N^{3/2}D)$ . The original attention layer does not occupy any other parameter space except for input data, while the surrogate attention block occupies the space of two Monarch matrices, i.e.,  $O(N^{3/2})$ .

### 5.2.3. FFN

The FFN layer consists of two linear layers and an activation function, with a total time complexity of  $O(ND^2)$  and space complexity of  $O(D^2)$ . Similar to linear layers, the surrogate FFN block reduces them to  $O(ND^{3/2})$  and  $O(D^{3/2})$ .

### 5.3. Trainability

In order to prove that Surrogate Attention Block is capable of being trained, it needs to be shown that it is a linear time-invariant (LTI) system, which can be described by the following equations:

$$\begin{aligned} x_{t+1} &= \mathbf{A}x_t + \mathbf{B}u_{t+1} \\ y_{t+1} &= \mathbf{C}x_{t+1} + \mathbf{D}u_{t+1} \end{aligned} \tag{7}$$

where  $\mathbf{A}$ ,  $\mathbf{B}$ ,  $\mathbf{C}$ , and  $\mathbf{D}$  are time-invariant matrices representing the system dynamics,  $x_t$  is the state vector at time  $t$ ,  $u_{t+1}$  is the input vector at time  $t+1$ ,  $y_{t+1}$  is the output vector at time  $t+1$ .

The relationship between Surrogate Attention Block and LTI systems is demonstrated in Appendix A.3.

Tasks	Datasets	Metrics	Series Length
Long-term Forecasting	ETT(4 subsets), Electricity, Traffic, Weather, Exchange, ILI	MSE, MAE, R2, DTW	96, 192, 336, 720 (ILI: 24, 36, 48, 60)
Short-term Forecasting	M4 (6 subsets)	SMAPE, MASE, OWA	6~48
Imputation	ETT (4 subsets), Electricity, Weather	MSE, MAE, R2	96
Classification	UEA (10 subsets)	Accuracy	29~1751
Anomaly Detection	SMD, MSL, SMAP, SWaT, PSM	Precision, Recall, F1-Score	100

Table 5: Summary of experiment benchmarks.

## 6. Experimental evaluations

### 6.1. Experimental Setup

**Benchmark:** In general, we refer to the experimental setup in TimesNet[62]. Two new metrics are added to the long-term forecasting task and the imputation task: R-Square (**R2**) and Dynamic Time Wrapping (**DTW**). R2 evaluates the goodness of fit of a model to the data. It quantifies the proportion of the variance in the dependent variable that is explained by the model. R-Square values range from 0 to 1, with higher values indicating that the model captures a larger portion of the variation in the data. It helps assess how well the model represents the underlying data patterns. DTW is a method used for comparing two time series with potentially different lengths and time axes. It determines the optimal alignment of elements in the two series, minimizing their paired distances. Therefore, DTW can be used for measuring the waveform similarity between two time series. Table 5 summarizes the datasets, metrics, and series length settings for the five tasks. More details can be found in the Appendix B.

**Baseline:** We extensively modify and compare all the widely recognized advanced *X-formers*, including Transformer[63], Informer[8], Autoformer[6], FEDformer[19], Pyraformer[22], Non-stationary Transformer[39] (abbreviated as NST), PatchTST[64], Crossformer[40] and iTransformer[50]. Details of these advanced *X-formers* can be found in Appendix B.2.

**Setup:** All datasets are divided chronologically into training, validation, and test sets in a ratio of 6:2:2. The hyperparameters in these baselines are their reported default settings.

**Platform:** All the models were trained and tested on two Nvidia RTX A6000 GPUs with 16 GB of RAM, which ensured that all models ran successfully without the limitation of hardware resources.

### 6.2. Main result

#### 6.2.1. Long-term Forecasting

Long-term forecasting plays a crucial role in weather forecasting, traffic and electricity consumption planning. We follow the benchmarks used in Autoformer[6], including ETT[8], Electricity[65], Traffic[66], Weather[67], Exchange Rate[68] and ILI[69], across a spectrum of five practical domains. The experimental results are shown in Table 6. For all 9 *X-formers*, the number of tasks with improvement higher than -5% exceeds 1/2 of the total number of tasks (each model has a total of 180 tasks, including *Avg*). For Transformer, Informer, Autoformer, Nonstationary Transformer, and PatchTST, this number is 2/3. This generally indicates that the use of structured matrix optimization for *X-formers* has almost

no significant negative impact on performance. The Transformer, Informer, and Autoformer have shown the best performance, with at least a moderate improvement in tasks being indicated by positive values. This suggests that structured matrices can not only improve efficiency across a wide range of tasks, but also effectively enhance the predictive capabilities of the models.

Models	Transformer				Informer				Autoformer				Crossformer				FEDformer				Pyraformer				NST				PatchTST								
	Metric	MSE	MAE	R2	DTW	MSE	MAE	R2	DTW	MSE	MAE	R2	DTW	MSE	MAE	R2	DTW	MSE	MAE	R2	DTW	MSE	MAE	R2	DTW	MSE	MAE	R2	DTW								
ETTH1	96	11.1	9.4	23.1	15.4	32.8	19.3	113.4	14.3	12.3	7.9	9.2	7.8	9.1	6.2	5.6	5.2	11.7	7.5	6.0	5.2	23.7	15.0	60.5	10.1	7.2	4.3	6.5	3.7	-1.1	0.8	-0.6	0.3	-2.6	-2.0	-1.4	-1.7
	192	11.1	9.9	31.9	12.3	27.1	15.2	239.5	8.1	6.9	3.8	5.8	4.4	-2.3	-2.2	-1.9	-1.7	11.5	5.6	-7.0	-2.9	14.3	7.4	50.1	0.2	3.9	-3.7	-4.9	-7.8	-2.8	0.6	-1.7	0.0	-0.2	-0.9	-0.1	-0.5
	336	9.0	10.0	93.1	5.4	22.2	11.8	710.0	0.2	-3.1	-1.4	-2.8	-0.4	12.7	9.2	29.9	13.9	15.9	9.0	-11.3	4.1	23.3	17.1	332.9	7.0	20.5	14.7	47.8	4.8	-3.1	0.4	-2.2	-0.2	0.5	0.0	0.4	-0.1
	720	-7.7	-8.9	-60.0	-1.0	14.8	8.2	172.4	0.0	-2.4	0.3	-2.1	1.4	-13.3	-9.6	-24.6	-3.9	15.9	-9.2	-12.9	-5.4	1.3	0.5	12.1	-2.1	7.4	4.6	13.3	-1.9	7.2	4.3	6.7	1.9	-3.4	-2.1	-2.7	-1.4
	Avg	5.9	5.1	231.5	8.0	24.2	13.6	308.8	5.6	3.4	2.6	2.5	3.3	1.5	0.9	2.2	3.4	-13.8	-7.8	-9.3	-4.4	15.7	10.0	113.9	3.8	4.2	2.8	12.4	-2.2	0.0	1.5	0.5	0.5	-1.4	-1.3	-1.0	-0.9
ETTH2	96	41.1	23.4	174.6	31.0	44.1	24.9	71.7	22.6	20.1	-11.2	-6.3	-3.9	0.1	4.0	0.1	-6.7	2.3	1.8	0.7	0.4	-53.0	-22.4	-171.7	-37.9	-3.1	0.8	-1.1	1.4	-2.9	-1.7	-0.7	-1.3	-3.8	-1.7	-0.9	-1.7
	192	64.0	40.4	81.9	44.1	10.3	3.3	14.1	-8.4	8.8	6.2	3.7	2.4	66.3	45.4	128.6	39.7	3.6	2.6	1.4	3.3	40.6	27.0	57.4	-9.3	7.5	3.5	-17.6	4.1	0.9	2.3	0.3	0.9	-4.8	-2.0	-1.6	-1.0
	336	37.9	22.9	59.4	23.9	24.7	13.8	35.3	14.1	0.6	2.0	0.3	3.8	-69.9	-28.8	-274.6	-22.8	6.0	2.2	2.8	3.0	36.0	18.2	53.1	-8.1	-4.7	-1.3	-2.8	-0.1	-2.5	-0.8	-0.9	-0.4	-5.0	-3.4	-1.9	1.1
	720	31.3	18.0	47.9	12.3	1.8	0.3	3.1	-7.9	12.4	8.4	6.7	9.3	-27.8	-14.0	-68.4	-4.0	-0.1	1.2	0.0	1.9	30.1	26.0	46.4	-31.9	0.2	0.3	0.1	0.4	-4.9	-2.9	-1.8	2.0				
	Avg	43.6	26.3	91.0	27.8	31.0	5.1	0.4	1.3	1.1	2.9	-7.8	1.6	-53.6	1.5	3.0	1.4	2.2	13.4	12.2	-3.7	-14.6	-3.8	-0.9	-7.6	0.4	-1.1	0.0	-0.3	-0.1	-4.6	-2.5	-1.5	0.1			
ETThm1	96	35.5	23.4	59.2	30.0	26.6	11.7	41.3	12.9	9.9	3.2	8.4	3.6	2.1	0.9	1.2	-1.2	-7.0	-3.6	-3.5	-1.8	9.6	0.1	10.7	-1.7	5.2	1.8	3.2	2.1	-1.1	-0.5	-0.5	-0.9	2.6	0.9	1.1	-0.6
	192	40.0	27.6	115.0	30.7	32.3	20.5	81.2	20.8	17.8	8.2	20.3	7.6	-9.7	-11.2	-6.1	-11.6	-1.5	-1.7	-1.0	-0.3	14.6	3.4	23.1	3.8	-15.0	-8.4	-11.2	-6.4	0.0	1.9	0.0	1.5	1.8	0.6	0.9	-0.6
	336	46.1	31.3	181.1	34.8	26.0	13.7	400.8	13.2	10.6	5.0	12.5	5.9	-29.0	-19.3	-26.8	-20.3	-7.2	-3.5	-5.0	-4.4	15.3	4.2	29.7	6.6	-14.4	-4.9	-15.1	-3.6	-1.8	0.5	-1.0	0.1	7.0	2.3	4.8	0.6
	720	39.5	24.5	622.9	26.6	30.9	18.0	386.3	15.4	13.0	5.9	13.9	3.5	-3.4	-1.1	-5.8	-2.1	-7.7	-4.1	-6.5	-5.6	34.1	13.8	94.1	13.3	19.6	7.6	35.3	7.8	-1.7	1.6	-1.2	1.3	3.0	1.2	2.5	-0.3
	Avg	40.3	26.7	652.1	30.5	28.9	15.9	227.4	15.6	12.8	5.6	13.8	5.1	-10.0	-7.7	-9.4	-8.8	-5.8	-3.2	-4.0	-3.0	18.4	5.4	251.1	5.5	-1.2	-1.0	3.0	0.0	-1.1	0.9	-0.7	0.5	3.6	1.2	2.3	-0.2
ETThm2	96	-65.7	-44.1	-24.5	-40.4	5.0	2.1	1.9	-10.0	-24.5	-13.1	-4.5	-8.3	2.1	-1.0	0.5	-1.7	-3.0	-1.2	-0.4	-2.3	-52.5	-34.6	-14.7	-38.9	17.8	8.0	3.3	6.7	1.3	0.1	0.2	-1.0	3.3	2.0	0.5	-0.1
	192	16.3	0.4	26.7	-3.0	15.0	5.6	13.8	-0.9	5.5	2.0	1.3	-0.1	-6.0	-8.5	-2.2	-6.5	-1.0	-0.3	-0.2	-1.7	-5.8	-8.0	-5.3	-7.4	11.0	3.7	6.8	0.5	-0.7	-0.5	0.1	-0.8	2.0	1.6	0.4	-0.8
	336	-21.0	-6.3	-98.5	-9.0	30.0	13.4	595.0	7.9	-4.4	-1.3	-1.3	-0.6	25.6	12.7	72.0	10.1	0.3	-0.5	0.1	-16.1	-16.2	-64.1	-12.5	-8.8	-14.6	-5.3	-7.4	1.3	0.6	0.3	1.1	-4.6	-1.8	-1.2	-0.8	
	720	-26.7	-14.7	-56.7	-18.7	18.9	10.8	32.1	10.3	-11.3	-7.9	-4.2	-4.3	43.5	21.4	65.5	13.7	-3.2	-0.9	-1.2	-2.8	36.0	18.3	66.7	-11.5	33.8	17.1	21.9	13.6	1.0	0.0	0.4	-1.0	-8.0	-3.4	-2.9	-1.8
	Avg	-24.3	-16.2	-38.3	-17.8	17.2	8.0	160.7	1.8	-8.7	-5.1	-2.2	-3.0	16.3	6.2	33.9	3.9	-1.7	-0.7	-0.4	-1.9	-8.8	-10.1	-4.3	-17.6	13.4	3.6	6.7	3.3	-1.1	0.0	0.3	-0.4	-1.8	-0.4	-0.8	-0.9
EXG	96	42.4	19.0	22.3	16.4	24.6	14.6	30.6	13.4	13.1	5.6	1.5	10.4	-24.5	-17.5	-4.2	-19.5	11.4	-4.9	-1.1	-8.9	7.2	4.7	2.8	-4.1	18.7	5.0	1.8	8.2	-1.3	-0.5	-0.1	-3.1	7.6	4.4	0.4	10.8
	192	-14.8	-11.4	-20.9	-0.5	-4.1	-3.8	-7.8	-6.0	-0.2	1.2	0.0	2.6	-138.3	-53.2	-52.3	-30.4	0.7	0.4	0.1	-2.8	4.5	1.1	8.5	-7.5	12.5	4.6	2.3	9.1	-4.9	-2.1	-0.6	-9.8	1.1	0.8	0.1	2.5
	336	16.5	0.2	56.0	3.6	12.3	2.7	335.7	3.6	6.7	4.1	2.6	4.6	9.6	3.8	26.9	-2.2	33.6	23.8	23.8	24.7	2.9	-4.2	11.4	-3.8	12.7	4.9	4.7	9.8	-0.7	0.4	-0.2	0.2	4.9	2.7	1.3	5.0
	720	48.6	28.8	132.6	19.8	45.7	28.7	114.9	18.3	-5.2	-1.8	-9.9	1.1	8.4	2.2	107.5	-5.5	17.0	11.7	108.1	15.3	27.2	13.2	102.0	-0.9	28.6	9.3	310.3	18.6	1.0	0.2	1.1	10.7	-2.8	-0.5	-3.1	-0.5
	Avg	23.2	9.2	47.5	9.8	19.6	10.6	118.4	7.3	3.6	2.3	-1.5	4.7	-36.2	-16.2	-19.5	-14.4	10.0	7.8	32.7	7.1	10.5	3.2	31.2	-4.1	18.1	6.0	79.8	11.4	-1.5	-0.5	0.1	-0.5	2.7	1.9	-0.3	4.5
ECL	96	-7.5	-3.8	-2.6	-3.5	1.6	0.6	0.8	-1.6	2.9	2.2	0.7	0.5	7.3	6.4	1.2	4.5	-10.2	-6.2	-2.5	-3.5	-6.1	-3.5	-2.4	-2.5	-13.9	-10.1	-2.8	-6.5	-6.3	-3.2	-1.4	-2.8	-33.5	-19.4	-5.7	-15.3
	192	-5.1	-5.0	-1.8	-2.1	-3.4	-2.4	-1.8	-2.5	6.5	4.7	1.9	3.0	-4.4	-2.7	-0.9	-1.6	-14.7	-8.5	-3.7	-7.5	-6.4	-3.9	-2.7	-3.3	-10.2	-7.8	-2.3	-4.9	-5.2	-3.2	-1.2	-2.5	-26.3	-15.3	-5.2	-12.5
	336	0.7	-1.8	0.3	-0.5	-1.3	-0.7	-0.7	-1.9	20.0	10.6	7.5	6.3	-	-	-	-	-5.9	-3.1	-1.8	-1.5	-4.3	-2.9	-1.9	-2.4	-12.1	-7.2	-3.0	-5.4	-4.2	-9.9	-1.0	-1.4	-27.1	-15.8	-5.8	-12.0
	720	-0.4	-1.3	-0.2	-0.7	6.8	3.4	4.8	-0.9	14.6	6.3	6.4	12.0	-	-	-	-	-9.2	-5.8	-3.3	-1.4	6.1	4.0	2.8	4.0	84.3	61.9	81.0	-273.4	-2.5	-1.8	-0.7	-2.9	-8.9	3.3	-3.0	-3.3
	Avg	-3.1	-3.0	-1.1	-1.7	0.9	0.2	-0.8	-1.7	11.0	6.0	4.1	5.5	-	-	-	-	-10.0	-5.9	-2.8	-3.5	-2.7	-1.6	-1.1	-0.1	12.0	9.2	20.0	-7.25	-4.6	-4.5	-1.1	-2.4	-24.0	-11.8	-4.9	-10.8
WTH	96	26.9	13.5	49.8	19.8	21.0	12.8	94.6	12.9	-6.5	-4.7	-5.1	-6.1	11.9	7.1	5.4	8.6	-11.2	-7.7	-6.9	-7.5	4.8	4.4	2.2	3.1	-8.3	-6.7	-4.0	-7.8	-7.7	-3.8	-3.4	-5.8	7.9	2.8	3.5	2.8
	192	38.1	21.3	679.8	24.6	3.2	0.7	43.7	-0.8																												

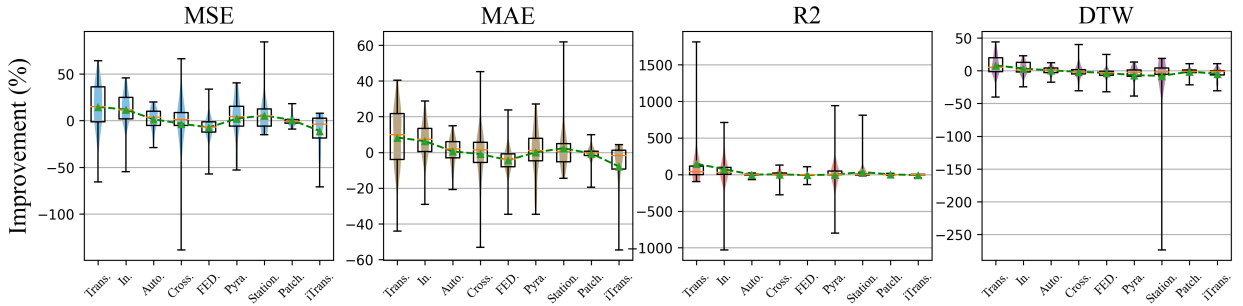


Figure 2: Box plots of statistical results on the distribution of **long-term forecasts** for each metric. The horizontal axis denotes the models, and the vertical axis is the percentage of lift after using the structured matrix. The width of the color blocks in the box indicates the density of the distribution. The green dashed line is the mean, and the orange dashed line is the median.

ness of our structured matrix optimization approach across different *X-former* architectures can be attributed to fundamental differences in their design philosophies and operational mechanisms. These models represent a new generation of transformers that have moved beyond the standard attention mechanisms found in traditional models such as the original Transformer, Informer, and Nonstationary Transformer.

These newer architectures often incorporate specialized components and processing strategies that are tailored to address specific challenges in time series forecasting. Common features among these models include:

- Advanced attention mechanisms: Many of these models use modified or enhanced attention techniques that deviate from the standard dot-product attention. These could include cross-dimensional, frequency-domain, or inverted attention mechanisms.
- Multi-resolution or hierarchical processing: Some of these architectures employ techniques to analyze data at multiple scales or in a hierarchical manner, which can be more efficient for capturing both long-term and short-term dependencies.

The presence of these advanced features may limit the additional benefits that can be gained from our structured matrix optimization approach. These architectures might already inherently capture some of the computational efficiencies that structured matrices provide in more standard models. Moreover, the complex interactions between these specialized components and structured matrices could potentially introduce unexpected behaviors or diminish the effectiveness of our optimization technique. It's important to note that our structured matrix optimization was primarily designed with traditional transformer architectures in mind. The more complex and specialized nature of these newer models may require a different approach to optimization, one that is more closely aligned with their unique operational principles.

The visualization in Figure 2 displays the distribution of data for each model, and Figure 3 illustrates the improvement of each model on different datasets. It is evident from this that almost all the improvements in *X-formers* have mean and median values above 0. This once again emphasizes the positive impact of structured matrices on predictive performance.

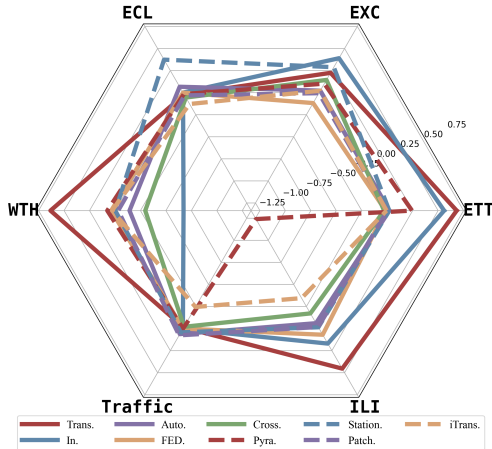


Figure 3: Comparison of performance improvement ratio after using structured matrices to enhance *X-formers* on five datasets on long-term forecasting tasks.

Table 7 presents a detailed comparison between the original models and their optimized counterparts in terms of parameters and FLOPS. The results highlight substantial improvements across various architectures, with the optimized models consistently achieving reductions in both model size and computational cost. On average, the optimizations lead to a 63.6% decrease in parameters and a 65.5% reduction in FLOPS, demonstrating the efficiency of the proposed approach. These results indicate that our method significantly enhances scalability and is particularly effective in improving X-former architectures.

Table 7: Comparison of model parameters and FLOPS reduction between original and optimized models using our method

		Trans.	In.	Auto.	FED.	Cross.	Pyra.	NST	Patch.	iTrans.
Paras (M)	Original	10.54	11.33	13.68	10.54	42.06	7.61	6.37	0.22	6.90
	Ours	2.66	4.50	6.87	2.67	31.04	2.36	1.12	0.09	1.65
	Improv.	74.7%	60.2%	49.8%	74.7%	26.2%	69.0%	82.4%	58.9%	76.0%
FLOPS (G)	Original	1.19	1.09	1.57	1.19	1.97	0.81	0.61	0.0025	0.53
	Ours	0.31	0.41	0.81	0.31	1.48	0.15	0.10	0.0010	0.09
	Improv.	74.1%	62.4%	48.2%	74.1%	24.6%	82.0%	83.0%	58.6%	82.4%

### 6.2.2. Short-term Forecasting

For short-term forecasting, the M4 datasets[70] are utilized. These datasets consist of univariate marketing data collected yearly, quarterly, and monthly, comprising 100,000 diverse time series gathered at various frequencies. Table 8 presents the experimental results of short-term forecasting tasks. The data in the table represents the percentage change in predictive performance of the model after applying structured matrix optimization, where positive numbers indicate improved performance. The visualization in Figure 4 displays the distribution of data for each model in Table 8. From Table 8 and Figure 4, it can be seen

Models	Trans.	In.	Auto.	FED.	Cross.	Pyra.	NST	PatchTST	iTrans.
Yearly	SMAPE	1.48%	2.22%	5.78%	-3.85%	12.23%	3.40%	13.19%	-0.46%
	MAPE	6.59%	1.08%	12.55%	-6.09%	-2.28%	10.74%	16.79%	2.01%
	MASE	2.18%	2.24%	8.24%	-2.45%	3.15%	8.48%	10.31%	-1.43%
	OWA	1.85%	2.20%	6.90%	-3.21%	7.76%	8.36%	11.79%	-1.01%
Quarterly	SMAPE	19.36%	2.01%	6.08%	-0.49%	1.33%	16.04%	16.33%	-0.74%
	MAPE	33.91%	2.03%	8.68%	0.62%	-5.12%	18.50%	19.07%	-0.46%
	MASE	29.30%	3.00%	6.84%	-1.12%	-1.05%	19.23%	19.16%	-0.25%
	OWA	25.23%	2.44%	6.43%	-0.74%	-0.07%	17.57%	17.75%	-0.45%
Monthly	SMAPE	3.06%	4.87%	0.87%	-0.33%	0.43%	10.39%	28.43%	-0.67%
	MAPE	3.45%	5.51%	0.02%	-0.35%	-3.73%	11.42%	29.09%	-1.90%
	MASE	-1.75%	8.25%	2.20%	0.09%	-0.57%	15.90%	38.58%	-0.21%
	OWA	-0.22%	6.62%	1.59%	-0.10%	-0.26%	13.21%	33.86%	-0.45%
Others	SMAPE	0.28%	11.14%	1.48%	0.04%	42.35%	10.90%	10.46%	-8.13%
	MAPE	0.20%	21.28%	5.21%	-2.21%	30.87%	13.54%	9.12%	-28.77%
	MASE	0.33%	4.58%	2.95%	-0.85%	31.42%	15.58%	15.55%	2.40%
	OWA	0.31%	7.94%	2.25%	-0.40%	36.91%	13.34%	13.09%	-2.81%
Weighted Average	SMAPE	6.48%	3.76%	3.19%	-1.23%	8.13%	9.84%	6.50%	-0.79%
	MAPE	11.31%	4.14%	5.38%	-1.66%	-1.28%	10.46%	10.31%	-1.20%
	MASE	5.61%	4.40%	5.55%	-1.30%	10.19%	10.77%	37.44%	-0.44%
	OWA	5.95%	4.04%	4.41%	-1.21%	9.42%	10.26%	23.47%	-0.70%

Table 8: Full results for the short-term forecasting task in the M4 dataset. Positive numbers indicate performance improvement, while negative numbers indicate the opposite, regardless of whether the evaluation metric is higher-the-better or lower-the-better.

that the adaptability of the structured matrix to short-term forecasting tasks is very good, with over 66% of tasks showing improved predictive performance, with a mean improvement of 5.35%.

### 6.2.3. Imputation

In real-world production scenarios, due to sensor or network failures, the collected time series data may be partially lost. Incomplete datasets can pose obstacles to downstream tasks, hence imputation is widely applied in practice. Experiments are carried out on ETT, Electricity and Weather datasets, where encountering the data-missing issue is frequent. To evaluate the model’s capability under varying levels of missing data, we randomly conceal time points at 12.5%, 25%, 37.5% and 50% ratios. Table 9 presents the experimental results of imputation tasks. The visualization in Figure 5 displays the distribution of data for each *X-former*. Positive advancements are evident across almost all 9 *X-formers*, with Autoformer showcasing the most significant improvement, averaging 50%. The result indicates that our method performs well on the imputation task and can capture temporal changes from incomplete time series.

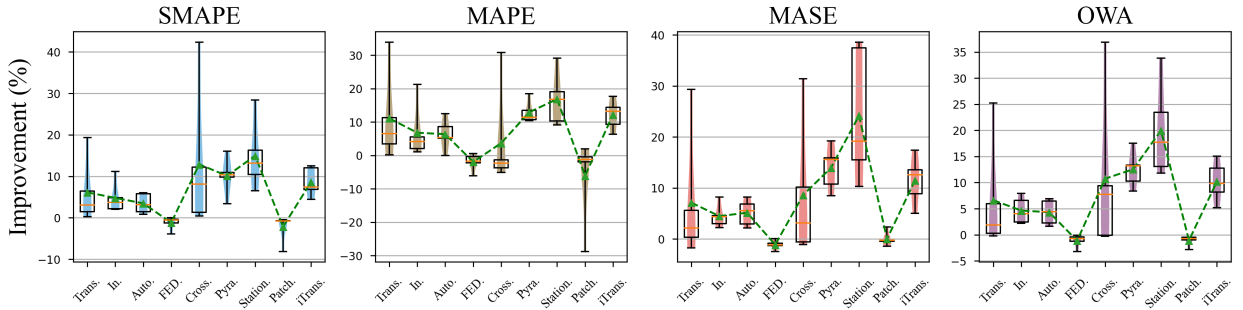


Figure 4: Box plots of statistical results on the distribution of **short-term forecasts** for each metric. The horizontal axis denotes the models, and the vertical axis is the percentage of lift after using the structured matrix. The width of the color blocks in the box indicates the density of the distribution. The green dashed line is the mean, and the orange dashed line is the median.

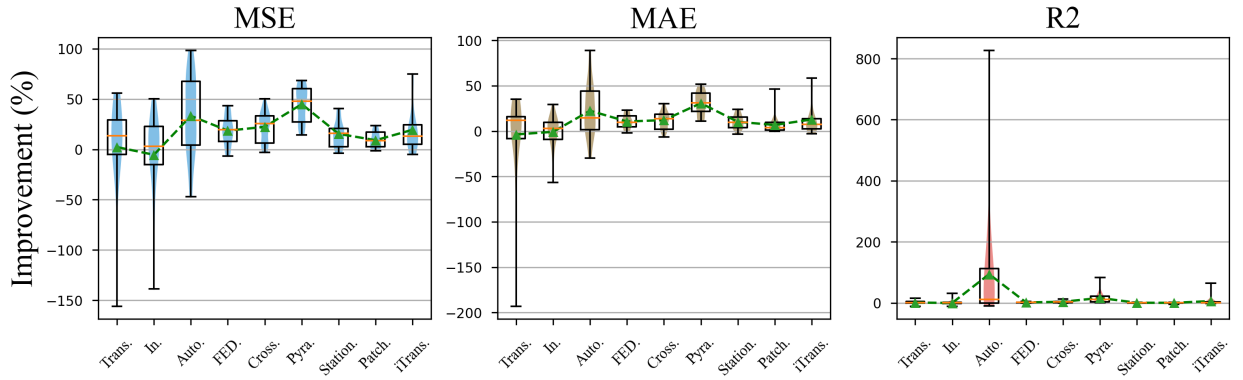


Figure 5: Box plots of statistical results for the distribution of **imputation** for each metric. The horizontal axis is the model and the vertical axis is the percentage of lift after using the structured matrix. The width of the color blocks in the box indicates the density of the distribution. The green dashed line is the mean and the orange dashed line is the median.

#### 6.2.4. Classification

We have selected 10 multidimensional datasets from the UEA time series classification repository[71], covering gesture, activity and audio recognition, heart rate monitoring for medical diagnosis, and other real-world tasks. Table 10 presents the experimental results of classification tasks. The visualization in Figure 6 displays the distribution of data for each model in Table 10. It is evident that Pyraformer’s optimization performance is lacking, resulting in an average decrease of 5.7% in classification accuracy. This decline is likely due to the sampling operations within Pyraformer’s pyramid structure, which may disrupt the information organization of the structured matrix, leading to the loss of crucial information required for accurate classification. Apart from Pyraformer, the performance of the other 8 *X-formers* is acceptable, with the worst one only decreasing the accuracy by 3.5% (iTransformer).

Models	Transformer			Informer			Autoformer			Crossformer			FEDformer			Pyraformer			NST			PatchTST			iTransformer			
	Metric	MSE	MAE	R2	MSE	MAE	R2	MSE	MAE	R2	MSE	MAE	R2	MSE	MAE	R2	MSE	MAE	R2	MSE	MAE	R2	MSE	MAE	R2	MSE	MAE	R2
ETTm1	0.125	28.06	11.61	2.43	24.89	9.33	2.30	6.86	2.74	0.72	-6.77	-2.19	-0.82	23.75	11.10	2.29	59.20	39.52	11.91	25.25	13.80	1.51	5.89	0.98	0.60	5.23	1.41	0.56
	0.25	32.40	15.78	4.26	23.78	10.91	3.10	17.54	8.19	2.57	-4.83	-0.31	-0.69	27.53	14.68	4.11	63.14	42.41	19.87	20.75	12.21	1.66	9.08	2.82	1.06	17.05	8.69	3.50
	0.375	35.84	18.15	6.40	16.21	8.74	2.60	18.70	10.81	3.93	-1.13	1.19	-0.19	27.04	14.95	5.83	44.70	28.62	14.10	21.57	12.37	2.29	10.44	3.74	1.46	3.96	2.23	1.06
	0.5	27.86	14.94	5.79	4.62	2.65	0.93	16.84	10.25	5.08	2.84	1.91	0.52	24.53	12.72	7.42	42.67	26.15	16.84	18.72	10.22	2.47	11.28	4.45	1.90	-4.95	-2.89	-1.91
ETTm2	0.125	51.40	31.89	15.45	14.60	7.39	4.24	76.37	54.02	114.10	8.02	2.55	0.79	32.55	16.58	4.62	66.85	45.28	29.92	10.10	6.60	0.31	0.35	-0.08	0.01	7.65	4.14	0.57
	0.25	24.69	14.67	6.44	50.27	29.34	31.60	20.02	7.35	4.14	16.31	9.21	1.95	37.91	20.67	8.64	55.47	37.76	21.69	12.59	8.77	0.44	1.95	0.76	0.08	6.51	2.94	0.61
	0.375	21.06	13.27	5.92	-18.29	-9.92	-5.01	30.28	14.79	9.95	20.95	11.76	3.09	35.66	19.49	11.57	53.71	38.04	36.49	13.03	8.65	0.53	2.67	1.39	0.13	11.55	5.38	1.40
	0.5	15.88	12.05	4.92	-35.67	-13.28	-10.23	27.51	13.98	13.17	26.73	16.55	4.53	29.09	15.24	13.60	67.06	48.05	83.85	11.33	6.85	0.52	2.98	1.75	0.16	32.46	16.64	7.39
ETTm3	0.125	52.19	31.11	2.31	35.23	20.77	1.44	47.21	27.68	67.59	21.50	9.46	1.17	35.03	19.83	1.77	45.21	27.29	2.24	33.47	19.55	0.91	11.45	3.93	0.51	-4.67	-2.14	-0.18
	0.25	43.57	26.36	2.30	27.25	14.87	1.50	66.95	44.09	152.50	34.15	17.49	2.30	32.79	18.57	2.47	48.64	31.51	3.16	39.50	23.84	1.43	19.62	9.00	1.01	3.56	1.85	0.23
	0.375	55.98	35.00	4.81	29.57	15.44	2.34	58.66	36.88	233.30	39.13	20.65	3.25	26.98	15.77	2.96	47.14	30.51	3.65	40.48	23.85	1.83	22.44	11.75	1.36	22.36	12.53	2.17
	0.5	24.41	14.66	1.42	22.34	10.89	2.12	69.12	46.03	826.61	43.43	22.86	4.28	22.82	12.53	3.96	49.19	33.24	4.88	36.92	21.07	2.01	23.80	12.93	1.66	29.85	17.72	4.72
ETTm2	0.125	-33.58	-7.78	-2.65	-138.43	-56.61	-10.59	75.60	49.89	106.20	19.33	9.43	1.02	50.34	30.09	4.25	68.43	51.89	21.80	19.31	17.37	0.29	2.59	0.86	0.05	13.08	6.06	0.53
	0.25	-24.42	-9.99	-2.48	-87.27	-35.94	-9.35	46.72	27.97	110.00	37.27	20.90	2.38	43.48	27.52	5.09	60.39	41.43	20.48	19.05	16.22	0.31	6.91	3.82	0.14	17.59	7.24	1.05
	0.375	-155.94	-65.80	-10.94	-66.33	-25.65	-10.46	63.15	40.38	215.53	41.04	23.30	3.56	37.79	23.91	6.24	60.82	43.56	27.06	19.04	15.02	0.35	7.99	4.77	0.18	22.10	11.25	1.84
	0.5	-134.49	-56.37	-10.17	-28.70	-14.14	-5.83	70.54	44.38	203.60	35.02	20.19	3.31	21.39	11.49	5.36	64.00	45.04	38.67	19.38	14.22	0.40	9.05	6.01	0.23	74.74	47.76	33.17
ECL	0.125	-3.39	-0.26	-0.57	-0.89	1.45	-0.15	-5.64	-2.68	-1.28	20.15	10.28	1.74	3.67	1.94	0.84	28.14	13.15	9.23	1.23	1.49	0.11	17.30	9.63	1.23	11.91	7.78	1.06
	0.25	-3.91	-0.21	-0.71	2.34	3.10	0.46	-4.36	-1.78	-1.13	21.51	11.63	2.16	3.21	1.63	0.85	28.79	14.43	10.20	1.13	1.66	0.10	18.17	10.73	1.56	16.71	10.26	2.00
	0.375	-4.81	-193.19	-0.93	3.42	3.12	0.75	-5.56	-2.14	-1.62	20.17	10.96	2.22	2.92	1.43	0.86	22.14	11.21	7.26	1.42	1.47	0.14	18.71	11.33	1.92	13.49	8.21	1.88
	0.5	-5.00	-0.60	-1.03	0.41	2.34	0.10	-3.40	-1.15	-1.12	17.94	9.25	2.21	2.51	1.19	0.84	21.67	10.81	7.42	1.92	1.60	0.21	17.29	10.48	2.12	2.56	2.39	0.37
WTH	0.125	-7.45	-10.29	-0.42	12.15	9.22	1.03	98.27	88.92	105.23	-0.77	0.95	-0.05	-3.17	-6.62	-0.25	24.90	25.92	1.74	-3.65	-3.51	-0.17	-1.46	0.68	-0.07	-1.14	0.17	-0.09
	0.25	-3.00	-9.40	-0.20	-0.45	-1.35	-0.02	92.96	76.09	111.52	7.05	5.69	0.59	7.99	4.43	0.99	25.04	24.16	2.14	4.46	5.13	0.26	1.82	3.86	0.12	32.20	31.85	4.31
	0.375	6.70	10.68	0.52	-6.50	-2.89	-0.52	-38.50	-27.37	-6.21	12.71	9.20	1.21	6.74	1.22	1.23	16.18	14.38	1.36	0.04	3.20	0.01	-0.67	-0.13	-0.06	59.52	48.65	19.20
	0.5	11.13	15.89	0.99	-14.11	-9.00	-1.28	-47.09	-29.85	-10.12	14.79	10.83	1.49	4.13	1.01	1.03	14.43	13.95	1.33	2.62	4.31	0.19	-1.30	46.42	-4.21	74.04	58.53	64.75
Avg		0.02%			-2.05%			50.03%			10.31%			12.84%			30.74%			8.80%			5.46%			12.86%		

Table 9: Full results for the imputation task. For brevity, we omit the percent signs (%) from the data. Randomly mask 12.5%, 25%, 37.5% and 50% time points to compare the model performance under different missing degrees.

### 6.2.5. Anomaly Detection

Similar to imputation tasks, the motivation for anomaly detection also arises from sensor failures, except that the failures do not result in data loss but rather in data anomalies. Anomalous data deviates significantly from the true values, which can severely impact the performance of prediction or classification tasks. Therefore, anomaly detection is crucial for industrial maintenance. We focus on unsupervised time series anomaly detection, specifically detecting anomalous time points. We compare models from five widely used anomaly detection benchmarks: SMD[72], MSL[73], SMAP[73], SWaT[74] and PSM[75], covering applications in service monitoring, space and earth exploration, and water treatment. Following the preprocessing method in Anomaly Transformer[76], we segment the dataset into contiguous, non-overlapping segments using a sliding window approach. Table 11 presents the experimental results of anomaly detection tasks. The visualization in Figure 7 displays the distribution of data for each model in Table 11. Except Transformer, the performance changes of other *X-formers* are within 4%. The worst-performing one is Autoformer, with an average performance decrease of only 3.2%. This may come from the need for *X-formers* in anomaly detection to identify rare abnormal time patterns. The attention mechanism calculates the similarity between each pair of time points, which may be dominated by the normal time points and dilute the focus of the attention mechanism, thus replacing the attention mechanism has little effect on the results.

On average, the use of structured matrices in all five tasks improved the performance of *X-formers*. (see Figure 8).

Datasets \ Models	Trans.	In.	Auto.	FED.	Cross.	Pyra.	NST	PatchTST	iTrans.
EthanolConcentration	5.3%	10.1%	-1.4%	-2.8%	12.7%	-9.6%	7.0%	4.3%	10.6%
FaceDetection	-2.4%	0.5%	24.7%	-2.9%	36.6%	0.8%	-1.0%	-3.2%	-1.6%
Handwriting	-15.0%	-9.6%	4.4%	5.5%	255.8%	-36.7%	-15.4%	-6.6%	-11.9%
Heartbeat	0.7%	-1.3%	-4.1%	0.7%	4.1%	-8.0%	-2.7%	0.0%	-5.9%
JapaneseVowels	1.1%	1.4%	0.9%	-0.8%	0.6%	3.8%	0.8%	0.3%	0.6%
PEMS-SF	2.1%	-2.7%	3.6%	-1.4%	340.0%	0.8%	13.4%	-2.1%	-2.1%
SelfRegulationSCP1	-1.1%	3.9%	46.0%	23.3%	4.3%	1.5%	2.7%	3.9%	-1.8%
SelfRegulationSCP2	-6.9%	-3.1%	-6.2%	-2.2%	4.1%	-6.2%	-5.3%	-3.2%	-7.1%
SpokenArabicDigits	-0.6%	-0.3%	0.2%	-0.3%	-0.4%	-0.7%	-0.5%	-0.3%	0.1%
UWaveGestureLibrary	-0.4%	-1.1%	25.5%	2.2%	8.3%	-6.5%	1.9%	-0.8%	-1.5%
Average	-2.5%	-1.4%	10.6%	2.7%	72.6%	-5.7%	-0.6%	-1.3%	-3.5%

Table 10: Full results for the classification task. \*. indicates the name of \*former. Positive numbers indicate performance improvement, while negative numbers indicate the opposite, regardless of whether the evaluation metric is higher-the-better or lower-the-better.

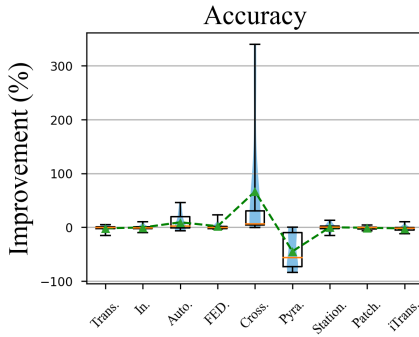


Figure 6: Box plots of statistical results on the distribution of **classification** for each metric. The horizontal axis denotes the models, and the vertical axis is the percentage of lift after using the structured matrix. The width of the color blocks in the box indicates the density of the distribution. The green dashed line is the mean, and the orange dashed line is the median.

### 6.3. Ablation study

To thoroughly evaluate the effectiveness and efficiency of our proposed approach, we conducted a comprehensive ablation study. This study aims to isolate and analyze the impact of various components and design choices in our model, providing insights into their individual and collective contributions to the overall performance. Our ablation experiments focus on three key aspects: Impact of Surrogate Blocks, Convergence and Trainability and Layer-wise Analysis.

Through these experiments, we aim to validate our design choices, quantify the improvements brought by each component, and provide a deeper understanding of our model's behavior under various conditions. The following subsections detail each part of our ablation study, presenting the experimental setup, results, and key findings.

Datasets	SMD			MSL			SMAP			SWaT			PSM			Avg F1
	Metrics	P	R	F1	P	R	F1	P	R	F1	P	R	F1	P	R	F1
Trans.	36.9%	221.0%	138.0%	0.9%	0.3%	0.6%	-2.5%	-16.8%	-11.4%	-1.9%	-5.0%	-3.6%	15.5%	-12.2%	-1.2%	23.9%
In.	0.6%	0.0%	0.3%	2.7%	2.0%	2.4%	-0.9%	-2.4%	-1.8%	-2.3%	-7.3%	-5.0%	0.2%	-4.0%	-2.3%	-1.2%
Auto.	-0.2%	-1.0%	-0.6%	-0.1%	4.2%	2.3%	-4.4%	-39.5%	-26.1%	2.1%	9.0%	5.8%	0.0%	0.1%	0.1%	-3.2%
FED.	0.1%	8.3%	4.6%	0.0%	0.2%	0.1%	-0.6%	0.3%	-0.1%	2.2%	9.0%	5.9%	0.0%	0.1%	0.0%	2.0%
Cross.	1.3%	2.9%	2.2%	1.5%	0.8%	1.1%	-0.9%	0.5%	0.0%	-1.2%	-5.6%	-3.6%	0.2%	-1.1%	-0.5%	-0.2%
Pyra.	3.0%	11.6%	7.7%	0.6%	-5.3%	-2.7%	-1.6%	-15.3%	-10.2%	-3.0%	-11.5%	-7.6%	0.4%	-6.0%	-3.5%	-2.9%
NST	1.6%	8.7%	5.5%	0.2%	-3.8%	-1.9%	-0.8%	-1.3%	-1.1%	-0.7%	-2.1%	-1.5%	1.5%	0.4%	1.0%	0.4%
PatchTST	0.3%	1.0%	0.7%	-0.2%	0.3%	0.1%	-0.1%	-1.3%	-0.8%	-0.1%	-0.7%	-0.4%	-0.5%	-4.6%	-2.7%	-0.6%
iTrans.	-0.3%	-1.3%	-0.9%	1.5%	0.8%	1.1%	-2.0%	-17.1%	-11.5%	0.1%	-1.8%	-0.9%	0.9%	9.7%	5.3%	-1.1%

Table 11: Full results for the anomaly detection task. The P, R and F1 represent precision, recall, and F1-score, respectively. F1-score is the harmonic mean of precision and recall. A higher value indicates a better performance.

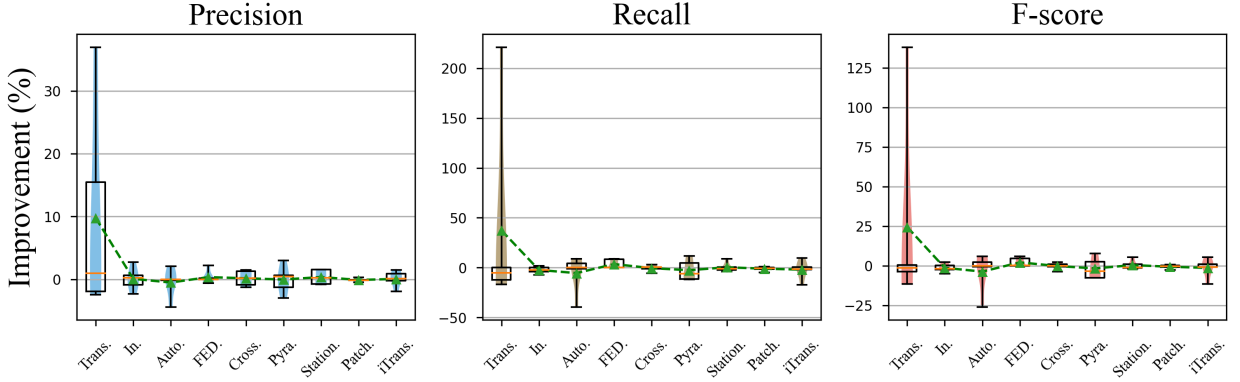


Figure 7: Box plots of statistical results on the distribution of **anomaly detection** for each metric. The horizontal axis denotes the models, and the vertical axis is the percentage of lift after using the structured matrix. The width of the color blocks in the box indicates the density of the distribution. The green dashed line is the mean, and the orange dashed line is the median.

### 6.3.1. Impact of Surrogate Blocks

To validate the effectiveness of the surrogate blocks we proposed, ablation experiments are conducted on the ETTh1 (series length = 96) dataset by only replacing the linear projection layer, feed-forward network layer, or self-attention layer on Transformer. Experimental results can be found in Table 12. Besides, we simultaneously counted the effects of the three surrogate blocks on the model size, and the results are also shown in Table 12. From Table 12 we can conclude that our proposed surrogate blocks have a positive impact on the prediction results while effectively reducing the size of the model, and no block is redundant.

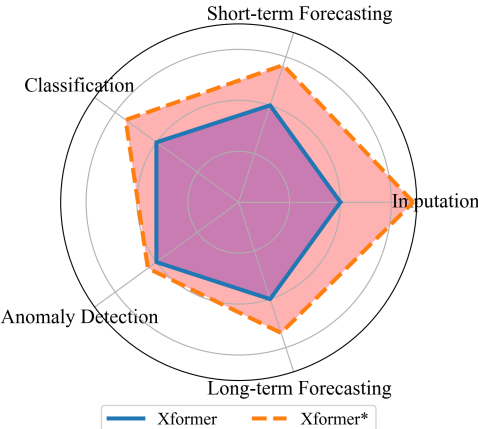


Figure 8: Radar chart of performance improvement on five tasks. The data represented by *Xformer* is the average of all *X-formers* experimental results. While *Xformer\** denotes the average experimental results after modifying *X-formers* using structured matrices. To standardize, the values of *Xformer* and *Xformer\** are divided by the value of *Xformer*.

	MSE		Model Size (MB)	
	Value	Impact	Value	Impact
Transformer	0.749	-	59.8	-
⊜ SAB	0.6401	-14.54%	55.7	-6.86%
⊜ SFB	0.7336	-2.06%	36.3	-39.30%

Table 12: The impact of the surrogate blocks on model performance and size.

### 6.3.2. Convergence and Trainability Analysis

We also compared the convergence and trainability of the model before and after using the structured matrix. Figure 9a shows the variation of losses of the model during the training process before and after the improvement. It is clear that the improved model achieves lower losses more quickly and with smaller fluctuations, indicating better convergence. Additionally, to validate our approach for making *X-formers* easier to train, we continuously reduced the size of the training set and repeated comparative experiments. We chose the Transformer model and conducted experiments on the electricity, exchange rate, and weather datasets. The experimental results are shown in Figure 9b, it can be seen that as the training set size decreases, the performance improvement ratio of the model optimized using structured matrices becomes increasingly significant. Therefore, it can be concluded that using structured matrices will make model training easier. In order to examine the inference time and GPU memory utilization of the model, we conducted a statistical analysis of the results of Transformer at various step lengths on the ETTh1 dataset. According to the results in Table 13, it is apparent that the model modified with SAB has faster inference speed and lower memory usage.

Series Length		96	192	336	720
Attn	Inf.(s/batch)	3.39	3.50	4.98	6.44
	Mem.(GB)	1.11	2.43	2.73	3.93
SAB	Inf.(s/batch)	<b>3.23</b>	<b>3.26</b>	<b>4.77</b>	<b>5.82</b>
	Mem.(GB)	<b>1.04</b>	<b>1.99</b>	<b>2.43</b>	<b>2.87</b>

Table 13: Comparison of inference time and GPU memory utilization with Attention blocks. **Bold** indicates better performance.

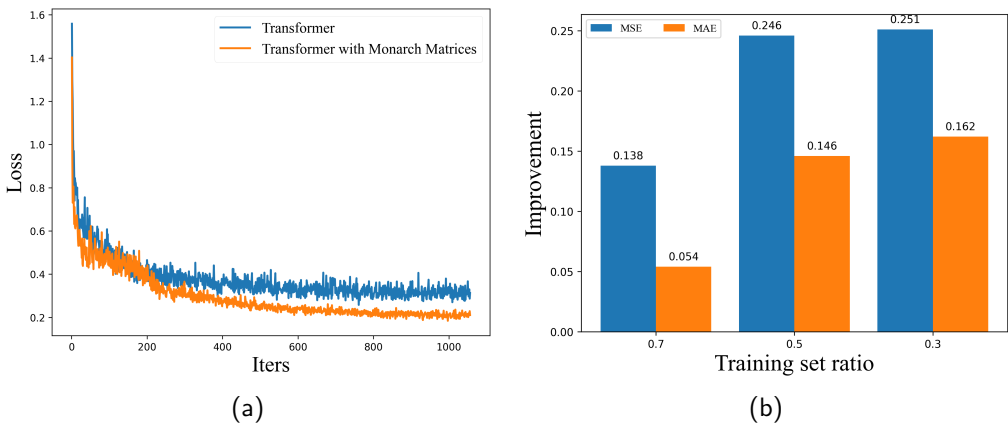


Figure 9: (a): Variation of loss with training iters. (b): Bar chart of experimental results with different training set sizes. The horizontal axis represents the proportion of training set size to the total dataset, while the vertical axis shows the performance improvement of the model using the structured matrix.

### 6.3.3. Layer-wise Analysis of Surrogate Attention Block

In addition, we also attempted to verify whether the surrogate attention block is useful at each layer. For the forecasting task, in a common experimental setup, two encoder layers and one decoder layer are used. Therefore, we chose Informer with three datasets and conducted control experiments for each layer, the results are shown in Figure 10. From the results, it is still the case that replacing the model in all layers performs the best.

### 6.4. Comparison experiment

Due to the equivalence between Monarch matrix multiplication and the convolution operation, we conducted an experiment to compare the performance of our structured matrix-based approach with a convolutional layer-based approach. Specifically, we attempted to replace the attention layer with either SAB or a convolutional layer. Table 14 shows the results of these two replacement methods on the Informer model. The data clearly demonstrates that our structured matrix-based approach yields significant performance improvements compared to the convolutional layer-based approach. This comparison highlights the potential advantages of using structured matrices over traditional convolutional operations

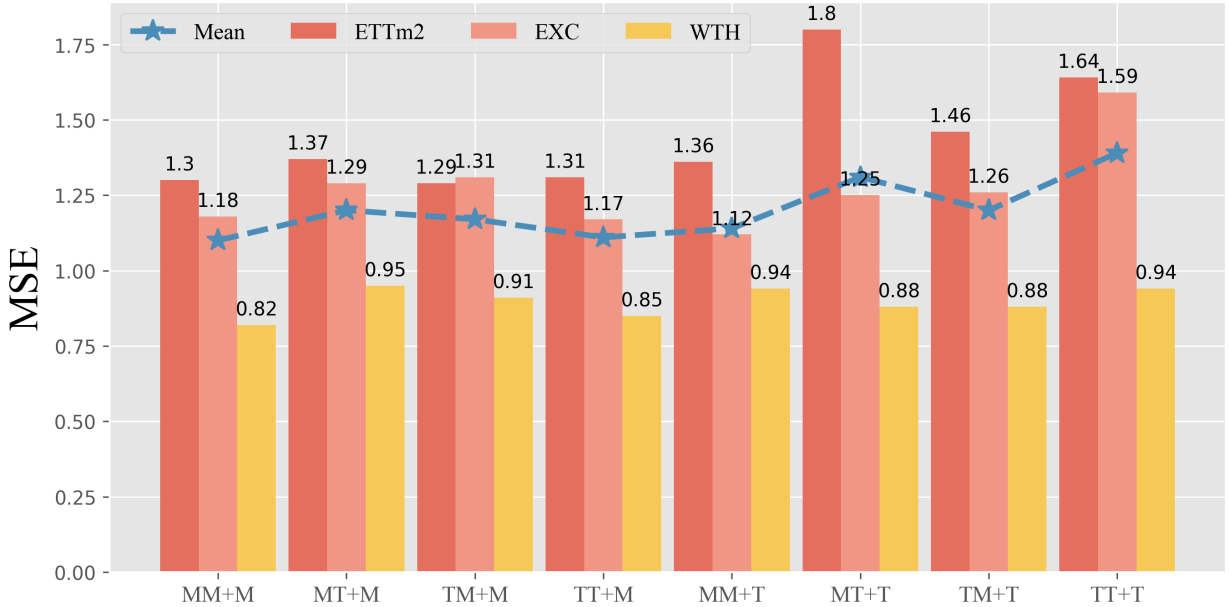


Figure 10: Comparison experiment results of replacing each layer with the Surrogate Attention Block.  $M$  represents the use of the Surrogate Attention Block, while  $T$  represents not using it. For example,  $MT+M$  denotes replacing the first layer of the encoder with the Surrogate Attention Block, while keeping the second layer of the encoder unchanged.

in certain deep learning architectures, particularly in the context of attention mechanisms in transformer-based models.

Since the  $O(n^{3/2})$  computational complexity brought by the structured matrix, it has led us to envision prediction horizons longer than 720. Therefore, we conducted experiments based on Informer on ETTh1 and ETTh2 datasets with prediction horizons of 1024 and 2048, respectively, as shown in Table 15. On a horizon of 1024, the enhanced Informer maintained better performance. On the horizon of 2048, the original Informer encountered a memory overflow issue, while the enhanced Informer was able to produce predictions normally. This indicates that for ultra-long sequence prediction tasks, models improved with structured matrices can have a clear advantage.

## 7. Conclusion, Discussion and Future Works

### 7.1. Conclusion

In this paper, our study introduces a groundbreaking structural innovation for *X-formers* tailored specifically for time series tasks. By designing the Surrogate Attention Block and Surrogate FFN Block built upon structured matrices, we endeavor to elevate efficiency without compromising on model performance. Crucially, we establish the Surrogate Attention Block’s equivalence to the conventional self-attention mechanism in terms of expressiveness and trainability, underscoring its suitability for LSTF tasks. Through comprehensive experimentation across nine Transformer-based models spanning five distinct time series

Metric	Informer (with CNN)		Informer (Ours)		Diff (CNN-Ours)/CNN	
	MSE	MAE	MSE	MAE	MSE	MAE
ETTm2	96	0.827	0.718	0.402	0.503	51.36% 29.85%
	192	1.149	0.835	0.623	0.622	45.78% 25.56%
	336	1.724	1.024	1.129	0.825	34.50% 19.49%
	720	3.107	1.325	3.062	1.338	1.45% -1.01%
EXC	96	0.884	0.741	0.723	0.680	18.24% 8.17%
	192	1.142	0.873	1.150	0.869	-0.70% 0.56%
	336	1.587	0.989	1.402	0.979	11.64% 1.02%
	720	2.487	1.315	1.457	0.963	41.43% 26.76%
WTH	96	0.629	0.583	0.372	0.427	40.84% 26.73%
	192	0.724	0.627	0.603	0.549	16.76% 12.30%
	336	0.784	0.654	0.851	0.671	-8.50% -2.61%
	720	1.033	0.759	1.878	1.032	-81.87% -36.08%
ILL	24	5.395	1.618	4.806	1.536	10.92% 5.08%
	36	4.972	1.518	4.715	1.497	5.16% 1.37%
	48	5.557	1.628	4.671	1.466	15.94% 9.93%
	60	5.818	1.675	5.263	1.554	9.54% 7.25%

Table 14: Comparison of Informer with self-attention layer replaced by convolution and Informer with self-attention layer replaced by our method on time series forecasting.

forecasting tasks, our findings showcase a remarkable average performance enhancement of 9.45%. Simultaneously, our framework achieves a substantial reduction in model size, slashing it by an impressive 46%, achieving the objective defined in Section 3.3.

## 7.2. Discussion

As indicated by the experimental results in Section 6, Surrogate Attention Block exhibits remarkable efficiency without compromising accuracy, enabling it to handle large-scale time series datasets efficiently. This ability stems from its ability to capture both short-term and long-term dependencies simultaneously and its equivalence with attention mechanisms.

As the core component of Surrogate Attention Block, Monarch matrices allow it to capture local dependencies akin to convolutional operations[59]. However, the Surrogate Attention Block performs better on time series tasks compared to convolutional layers. This is because convolution can only capture local dependencies, whereas the Surrogate Attention Block can also capture global dependencies (i.e. long-term dependencies, as proved in Section 5.1) that are also important in time series tasks.

Through inspecting the experimental results, compared to the other 8 *X-formers*, the Surrogate Attention Block shows a significant improvement in performance on the Vanilla Transformer. Furthermore, some works replacing attention mechanisms with simpler op-

		Informer		Informer <sup>*</sup>	
Datasets/Metrics		MSE	MAE	MSE	MAE
ETTh1	1024	1.284	0.931	<b>1.269</b>	<b>0.907</b>
	2048	-	-	<b>1.278</b>	<b>0.909</b>
ETTh2	1024	3.408	1.584	<b>3.395</b>	<b>1.581</b>
	2048	-	-	<b>2.689</b>	<b>1.285</b>

Table 15: The prediction results on the length of the ultra-long sequence. Where *Informer<sup>\*</sup>* represents the modified *Informer* with structured matrices. **Bold** indicates a better result. - indicates the result cannot be obtained due to memory overflow.

erators such as convolution, like Autoformer[6], have achieved better performance as well. These observations suggest that the pure self-attention mechanism in the Vanilla Transformer has limited effectiveness in time series compared to the Surrogate Attention Block and other special attention blocks in *X-formers*. This aligns with the conclusion in [77].

### 7.3. Future Works

The intuition derived from the discussion suggests a promising direction for future research that involves delving into the causative capabilities of attention mechanisms in time series forecasting. Examining how these mechanisms perceive causal connections within temporal data could unveil fresh perspectives and enhancements in forecasting precision. Subsequently, efforts can be made to decrease the dependence on self-attention mechanisms in time series forecasting, while crafting more straightforward yet efficient forecasting models that could offer advantages like decreased computational intricacy and enhanced scalability.

## References

- [1] A. Vaswani, P. Ramachandran, A. Srinivas, N. Parmar, B. A. Hechtman, J. Shlens, Scaling local self-attention for parameter efficient visual backbones, in: IEEE Conference on Computer Vision and Pattern Recognition, CVPR 2021, virtual, June 19-25, 2021, Computer Vision Foundation / IEEE, 2021, pp. 12894–12904.
- [2] L. Liu, Z. Qu, Z. Chen, Y. Ding, Y. Xie, Transformer acceleration with dynamic sparse attention, CoRR abs/2110.11299 (2021). [arXiv:2110.11299](https://arxiv.org/abs/2110.11299)  
URL <https://arxiv.org/abs/2110.11299>
- [3] J. Cordonnier, A. Loukas, M. Jaggi, On the relationship between self-attention and convolutional layers, in: 8th International Conference on Learning Representations, ICLR 2020, Addis Ababa, Ethiopia, April 26-30, 2020, OpenReview.net, 2020.  
URL <https://openreview.net/forum?id=HJ1nC1rKPB>
- [4] Q. Han, Z. Fan, Q. Dai, L. Sun, M. Cheng, J. Liu, J. Wang, On the connection between local attention and dynamic depth-wise convolution, in: The Tenth International Conference on Learning Representations, ICLR 2022, Virtual Event, April 25-29, 2022, OpenReview.net, 2022.  
URL [https://openreview.net/forum?id=L3\\_SsSNMmy](https://openreview.net/forum?id=L3_SsSNMmy)
- [5] X. Zhao, P. Zhang, F. Song, C. Ma, G. Fan, Y. Sun, Y. Feng, G. Zhang, Prior attention network for multi-lesion segmentation in medical images, IEEE Transactions on Medical Imaging 41 (12) (2022) 3812–3823.

- [6] H. Wu, J. Xu, J. Wang, M. Long, Autoformer: Decomposition transformers with auto-correlation for long-term series forecasting, in: M. Ranzato, A. Beygelzimer, Y. Dauphin, P. Liang, J. W. Vaughan (Eds.), Advances in Neural Information Processing Systems, Vol. 34, Curran Associates, Inc., 2021, pp. 22419–22430.
- [7] S. Wang, B. Z. Li, M. Khabsa, H. Fang, H. Ma, Linformer: Self-attention with linear complexity, CoRR abs/2006.04768 (2020).
- [8] H. Zhou, S. Zhang, J. Peng, S. Zhang, J. Li, H. Xiong, W. Zhang, Informer: Beyond efficient transformer for long sequence time-series forecasting, in: Thirty-Fifth AAAI Conference on Artificial Intelligence, AAAI 2021, Thirty-Third Conference on Innovative Applications of Artificial Intelligence, IAAI 2021, The Eleventh Symposium on Educational Advances in Artificial Intelligence, EAAI 2021, Virtual Event, February 2-9, 2021, AAAI Press, 2021, pp. 11106–11115.
- [9] S. Li, X. Jin, Y. Xuan, X. Zhou, W. Chen, Y.-X. Wang, X. Yan, Enhancing the locality and breaking the memory bottleneck of transformer on time series forecasting, in: H. Wallach, H. Larochelle, A. Beygelzimer, F. d'Alché-Buc, E. Fox, R. Garnett (Eds.), Advances in Neural Information Processing Systems, Vol. 32, Curran Associates, Inc., 2019.
- [10] U. Köster, T. Webb, X. Wang, M. Nassar, A. K. Bansal, W. Constable, O. Elibol, S. Gray, S. Hall, L. Hornof, et al., Flexpoint: An adaptive numerical format for efficient training of deep neural networks, Advances in neural information processing systems 30 (2017).
- [11] B. Jacob, S. Kligys, B. Chen, M. Zhu, M. Tang, A. Howard, H. Adam, D. Kalenichenko, Quantization and training of neural networks for efficient integer-arithmetic-only inference, in: Proceedings of the IEEE conference on computer vision and pattern recognition, 2018, pp. 2704–2713.
- [12] S. Zhou, Y. Wu, Z. Ni, X. Zhou, H. Wen, Y. Zou, Dorefa-net: Training low bitwidth convolutional neural networks with low bitwidth gradients, arXiv preprint arXiv:1606.06160 (2016).
- [13] G. Hinton, O. Vinyals, J. Dean, Distilling the knowledge in a neural network, arXiv preprint arXiv:1503.02531 (2015).
- [14] J. Ba, R. Caruana, Do deep nets really need to be deep?, Advances in neural information processing systems 27 (2014).
- [15] Y. LeCun, J. Denker, S. Solla, Optimal brain damage, Advances in neural information processing systems 2 (1989).
- [16] S. Han, J. Pool, J. Tran, W. Dally, Learning both weights and connections for efficient neural network, Advances in neural information processing systems 28 (2015).
- [17] G. Zerveas, S. Jayaraman, D. Patel, A. Bhamidipaty, C. Eickhoff, A transformer-based framework for multivariate time series representation learning, in: F. Zhu, B. C. Ooi, C. Miao (Eds.), KDD '21: The 27th ACM SIGKDD Conference on Knowledge Discovery and Data Mining, Virtual Event, Singapore, August 14-18, 2021, ACM, 2021, pp. 2114–2124.
- [18] B. Lim, S. O. Arik, N. Loeff, T. Pfister, Temporal fusion transformers for interpretable multi-horizon time series forecasting, International Journal of Forecasting 37 (4) (2021) 1748–1764.
- [19] T. Zhou, Z. Ma, Q. Wen, X. Wang, L. Sun, R. Jin, FEDformer: Frequency enhanced decomposed transformer for long-term series forecasting, in: K. Chaudhuri, S. Jegelka, L. Song, C. Szepesvari, G. Niu, S. Sabato (Eds.), Proceedings of the 39th International Conference on Machine Learning, Vol. 162 of Proceedings of Machine Learning Research, PMLR, 2022, pp. 27268–27286.
- [20] S. Tonekaboni, S. Joshi, K. Campbell, D. Duvenaud, A. Goldenberg, What went wrong and when? instance-wise feature importance for time-series black-box models, in: H. Larochelle, M. Ranzato, R. Hadsell, M. Balcan, H. Lin (Eds.), Advances in Neural Information Processing Systems 33: Annual Conference on Neural Information Processing Systems 2020, NeurIPS 2020, December 6-12, 2020, virtual, 2020.
- [21] Y. Cheng, R. Yang, T. Xiao, Z. Li, J. Suo, K. He, Q. Dai, CUTS: neural causal discovery from irregular time-series data, in: The Eleventh International Conference on Learning Representations, ICLR 2023, Kigali, Rwanda, May 1-5, 2023, OpenReview.net, 2023.
- [22] S. Liu, H. Yu, C. Liao, J. Li, W. Lin, A. X. Liu, S. Dustdar, Pyraformer: Low-complexity pyramidal attention for long-range time series modeling and forecasting, in: The Tenth International Conference

on Learning Representations, ICLR 2022, Virtual Event, April 25-29, 2022, OpenReview.net, 2022.

[23] Z. Dai, H. Liu, Q. V. Le, M. Tan, Coatnet: Marrying convolution and attention for all data sizes, in: M. Ranzato, A. Beygelzimer, Y. N. Dauphin, P. Liang, J. W. Vaughan (Eds.), Advances in Neural Information Processing Systems 34: Annual Conference on Neural Information Processing Systems 2021, NeurIPS 2021, December 6-14, 2021, virtual, 2021, pp. 3965–3977.

[24] Z. Yang, W. Yan, X. Huang, L. Mei, Adaptive temporal-frequency network for time-series forecasting, *IEEE Trans. Knowl. Data Eng.* 34 (4) (2022) 1576–1587. doi:10.1109/TKDE.2020.3003420. URL <https://doi.org/10.1109/TKDE.2020.3003420>

[25] L. Shen, Y. Wang, Tcct: Tightly-coupled convolutional transformer on time series forecasting, *Neurocomputing* 480 (2022) 131–145.

[26] Y. Zhao, Z. Ma, T. Zhou, L. Sun, M. Ye, Y. Qian, Gcformer: An efficient framework for accurate and scalable long-term multivariate time series forecasting, *CoRR* abs/2306.08325 (2023). arXiv: 2306.08325.

[27] L. donghao, wang xue, ModernTCN: A modern pure convolution structure for general time series analysis, in: The Twelfth International Conference on Learning Representations, 2024. URL <https://openreview.net/forum?id=vpJMJerXHU>

[28] G. Woo, C. Liu, D. Sahoo, A. Kumar, S. C. H. Hoi, Etsformer: Exponential smoothing transformers for time-series forecasting, *CoRR* abs/2202.01381 (2022).

[29] A. M. Abdelhakim, M. Saad, M. Sayed, H. I. Saleh, Optimized svd-based robust watermarking in the fractional fourier domain, *Multimedia Tools and Applications* 77 (2018) 27895–27917.

[30] T. Braconnier, M. Ferrier, J.-C. Jouhaud, M. Montagnac, P. Sagaut, Towards an adaptive pod/svd surrogate model for aeronautic design, *Computers & Fluids* 40 (1) (2011) 195–209.

[31] J. Zhang, Q. Lei, I. Dhillon, Stabilizing gradients for deep neural networks via efficient svd parameterization, in: International Conference on Machine Learning, PMLR, 2018, pp. 5806–5814.

[32] K. Devarajan, Nonnegative matrix factorization: an analytical and interpretive tool in computational biology, *PLoS computational biology* 4 (7) (2008) e1000029.

[33] X. Lin, P. C. Boutrous, Optimization and expansion of non-negative matrix factorization, *BMC bioinformatics* 21 (1) (2020) 1–10.

[34] M. Aharon, M. Elad, A. Bruckstein, K-svd: An algorithm for designing overcomplete dictionaries for sparse representation, *IEEE Transactions on signal processing* 54 (11) (2006) 4311–4322.

[35] H. Lee, A. Battle, R. Raina, A. Ng, Efficient sparse coding algorithms, *Advances in neural information processing systems* 19 (2006).

[36] H. He, H. Daume III, J. M. Eisner, Learning to search in branch and bound algorithms, *Advances in neural information processing systems* 27 (2014).

[37] E. Sprangle, R. S. Chappell, M. Alsup, Y. N. Patt, The agree predictor: A mechanism for reducing negative branch history interference, in: Proceedings of the 24th annual international symposium on Computer architecture, 1997, pp. 284–291.

[38] D. Du, B. Su, Z. Wei, Preformer: Predictive transformer with multi-scale segment-wise correlations for long-term time series forecasting, in: ICASSP 2023 - 2023 IEEE International Conference on Acoustics, Speech and Signal Processing (ICASSP), 2023, pp. 1–5.

[39] Y. Liu, H. Wu, J. Wang, M. Long, Non-stationary transformers: Exploring the stationarity in time series forecasting, in: S. Koyejo, S. Mohamed, A. Agarwal, D. Belgrave, K. Cho, A. Oh (Eds.), *Advances in Neural Information Processing Systems*, Vol. 35, Curran Associates, Inc., 2022, pp. 9881–9893.

[40] Y. Zhang, J. Yan, Crossformer: Transformer utilizing cross-dimension dependency for multivariate time series forecasting, in: The Eleventh International Conference on Learning Representations, 2023.

[41] L. Shen, Y. Wei, Y. Wang, H. Qiu, Take an irregular route: Enhance the decoder of time-series forecasting transformer, *IEEE Internet of Things Journal* (2023) 1–1.

[42] Y. Li, X. Lu, H. Xiong, J. Tang, J. Su, B. Jin, D. Dou, Towards long-term time-series forecasting: Feature, pattern, and distribution, in: 39th IEEE International Conference on Data Engineering, ICDE 2023, Anaheim, CA, USA, April 3-7, 2023, IEEE, 2023, pp. 1611–1624.

[43] J. Jiang, C. Han, W. X. Zhao, J. Wang, Pdformer: Propagation delay-aware dynamic long-range

transformer for traffic flow prediction, in: B. Williams, Y. Chen, J. Neville (Eds.), Thirty-Seventh AAAI Conference on Artificial Intelligence, AAAI 2023, Thirty-Fifth Conference on Innovative Applications of Artificial Intelligence, IAAI 2023, Thirteenth Symposium on Educational Advances in Artificial Intelligence, EAAI 2023, Washington, DC, USA, February 7-14, 2023, AAAI Press, 2023, pp. 4365–4373.

[44] K. Madhusudhanan, J. Burchert, N. Duong-Trung, S. Born, L. Schmidt-Thieme, Yformer: U-net inspired transformer architecture for far horizon time series forecasting, CoRR abs/2110.08255 (2021). [arXiv:2110.08255](https://arxiv.org/abs/2110.08255).

[45] W. Chen, W. Wang, B. Peng, Q. Wen, T. Zhou, L. Sun, Learning to rotate: Quaternion transformer for complicated periodical time series forecasting, in: Proceedings of the 28th ACM SIGKDD Conference on Knowledge Discovery and Data Mining, KDD '22, Association for Computing Machinery, New York, NY, USA, 2022, p. 146–156.

[46] S. Wu, X. Xiao, Q. Ding, P. Zhao, Y. Wei, J. Huang, Adversarial sparse transformer for time series forecasting, in: H. Larochelle, M. Ranzato, R. Hadsell, M. Balcan, H. Lin (Eds.), Advances in Neural Information Processing Systems, Vol. 33, Curran Associates, Inc., 2020, pp. 17105–17115.

[47] J. Grigsby, Z. Wang, Y. Qi, Long-range transformers for dynamic spatiotemporal forecasting, CoRR abs/2109.12218 (2021). [arXiv:2109.12218](https://arxiv.org/abs/2109.12218).

[48] X. Zhang, X. Jin, K. Gopalswamy, G. Gupta, Y. Park, X. Shi, H. Wang, D. M. Robinson, Y. B. Wang, First de-trend then attend: Rethinking attention for time-series forecasting, in: NeurIPS 2022 Workshop on All Things Attention: Bridging Different Perspectives on Attention, 2022.

[49] O. Nivron, R. Parthipan, D. J. Wischik, Taylorformer: Probabilistic predictions for time series and other processes, CoRR abs/2305.19141 (2023). [arXiv:2305.19141](https://arxiv.org/abs/2305.19141).

[50] Y. Liu, T. Hu, H. Zhang, H. Wu, S. Wang, L. Ma, M. Long, itransformer: Inverted transformers are effective for time series forecasting, CoRR abs/2310.06625 (2023). [arXiv:2310.06625](https://arxiv.org/abs/2310.06625), doi:10.48550/ARXIV.2310.06625.  
URL <https://doi.org/10.48550/arXiv.2310.06625>

[51] V. Sindhwani, T. N. Sainath, S. Kumar, Structured transforms for small-footprint deep learning, in: C. Cortes, N. D. Lawrence, D. D. Lee, M. Sugiyama, R. Garnett (Eds.), Advances in Neural Information Processing Systems 28: Annual Conference on Neural Information Processing Systems 2015, December 7-12, 2015, Montreal, Quebec, Canada, 2015, pp. 3088–3096.

[52] M. Moczulski, M. Denil, J. Appleyard, N. de Freitas, ACDC: A structured efficient linear layer, in: Y. Bengio, Y. LeCun (Eds.), 4th International Conference on Learning Representations, ICLR 2016, San Juan, Puerto Rico, May 2-4, 2016, Conference Track Proceedings, 2016.

[53] Q. Le, T. Sarlos, A. Smola, Fastfood - computing hilbert space expansions in loglinear time, in: S. Dasgupta, D. McAllester (Eds.), Proceedings of the 30th International Conference on Machine Learning, Vol. 28 of Proceedings of Machine Learning Research, PMLR, Atlanta, Georgia, USA, 2013, pp. 244–252.

[54] T. Dao, N. S. Sohoni, A. Gu, M. Eichhorn, A. Blonder, M. Leszczynski, A. Rudra, C. Ré, Kaleidoscope: An efficient, learnable representation for all structured linear maps, in: 8th International Conference on Learning Representations, ICLR 2020, Addis Ababa, Ethiopia, April 26-30, 2020, OpenReview.net, 2020.

[55] D. Y. Fu, S. Arora, J. Grogan, I. Johnson, S. Eyuboglu, A. W. Thomas, B. Spector, M. Poli, A. Rudra, C. Ré, Monarch mixer: A simple sub-quadratic gemm-based architecture, CoRR abs/2310.12109 (2023). [arXiv:2310.12109](https://arxiv.org/abs/2310.12109), doi:10.48550/ARXIV.2310.12109.  
URL <https://doi.org/10.48550/arXiv.2310.12109>

[56] E. Konstantinidis, Y. Cotronis, A practical performance model for compute and memory bound GPU kernels, in: M. Daneshtalab, M. Aldinucci, V. Leppänen, J. Lilius, M. Brorsson (Eds.), 23rd Euromicro International Conference on Parallel, Distributed, and Network-Based Processing, PDP 2015, Turku, Finland, March 4-6, 2015, IEEE Computer Society, 2015, pp. 651–658.

[57] T. Dao, B. Chen, N. S. Sohoni, A. D. Desai, M. Poli, J. Grogan, A. Liu, A. Rao, A. Rudra, C. Ré, Monarch: Expressive structured matrices for efficient and accurate training, in: International Con-

ference on Machine Learning, ICML 2022, 17-23 July 2022, Baltimore, Maryland, USA, Vol. 162 of Proceedings of Machine Learning Research, PMLR, 2022, pp. 4690–4721.  
 URL <https://proceedings.mlr.press/v162/dao22a.html>

[58] M. Poli, S. Massaroli, E. Nguyen, D. Y. Fu, T. Dao, S. Baccus, Y. Bengio, S. Ermon, C. Ré, Hyena hierarchy: Towards larger convolutional language models, in: A. Krause, E. Brunskill, K. Cho, B. Engelhardt, S. Sabato, J. Scarlett (Eds.), International Conference on Machine Learning, ICML 2023, 23-29 July 2023, Honolulu, Hawaii, USA, Vol. 202 of Proceedings of Machine Learning Research, PMLR, 2023, pp. 28043–28078.  
 URL <https://proceedings.mlr.press/v202/poli23a.html>

[59] D. Y. Fu, T. Dao, K. K. Saab, A. W. Thomas, A. Rudra, C. Ré, Hungry hungry hippos: Towards language modeling with state space models, in: The Eleventh International Conference on Learning Representations, ICLR 2023, Kigali, Rwanda, May 1-5, 2023, OpenReview.net, 2023.  
 URL <https://openreview.net/pdf?id=COZDy0WYGg>

[60] D. Y. Fu, E. L. Epstein, E. Nguyen, A. W. Thomas, M. Zhang, T. Dao, A. Rudra, C. Ré, Simple hardware-efficient long convolutions for sequence modeling, in: A. Krause, E. Brunskill, K. Cho, B. Engelhardt, S. Sabato, J. Scarlett (Eds.), International Conference on Machine Learning, ICML 2023, 23-29 July 2023, Honolulu, Hawaii, USA, Vol. 202 of Proceedings of Machine Learning Research, PMLR, 2023, pp. 10373–10391.  
 URL <https://proceedings.mlr.press/v202/fu23a.html>

[61] Y. Wang, J. Peng, X. Wang, Z. Zhang, J. Duan, Replacing self-attentions with convolutional layers in multivariate long sequence time-series forecasting, *Appl. Intell.* 54 (1) (2024) 522–543.

[62] H. Wu, T. Hu, Y. Liu, H. Zhou, J. Wang, M. Long, Timesnet: Temporal 2d-variation modeling for general time series analysis, in: The Eleventh International Conference on Learning Representations, ICLR 2023, Kigali, Rwanda, May 1-5, 2023, OpenReview.net, 2023.

[63] A. Vaswani, N. Shazeer, N. Parmar, J. Uszkoreit, L. Jones, A. N. Gomez, L. Kaiser, I. Polosukhin, Attention is all you need, in: I. Guyon, U. von Luxburg, S. Bengio, H. M. Wallach, R. Fergus, S. V. N. Vishwanathan, R. Garnett (Eds.), Advances in Neural Information Processing Systems 30: Annual Conference on Neural Information Processing Systems 2017, December 4-9, 2017, Long Beach, CA, USA, 2017, pp. 5998–6008.

[64] Y. Nie, N. H. Nguyen, P. Sinthong, J. Kalagnanam, A time series is worth 64 words: Long-term forecasting with transformers, CoRR abs/2211.14730 (2022). [arXiv:2211.14730](https://arxiv.org/abs/2211.14730), doi:10.48550/ARXIV.2211.14730.  
 URL <https://doi.org/10.48550/arXiv.2211.14730>

[65] UCI, Electricity, <https://archive.ics.uci.edu/ml/datasets/ElectricityLoadDiagrams20112014>.

[66] PeMS, Traffic, <http://pems.dot.ca.gov/>.

[67] Wetterstation, Weather, <https://www.bgc-jena.mpg.de/wetter/>.

[68] G. Lai, W. Chang, Y. Yang, H. Liu, Modeling long- and short-term temporal patterns with deep neural networks, in: K. Collins-Thompson, Q. Mei, B. D. Davison, Y. Liu, E. Yilmaz (Eds.), The 41st International ACM SIGIR Conference on Research & Development in Information Retrieval, SIGIR 2018, Ann Arbor, MI, USA, July 08-12, 2018, ACM, 2018, pp. 95–104.

[69] CDC, Illness, <https://gis.cdc.gov/grasp/fluview/fluportaldashboard.html>.

[70] Spyros Makridakis, M4 dataset (2018).  
 URL <https://github.com/M4Competition/M4-methods/tree/master/Dataset>

[71] A. J. Bagnall, H. A. Dau, J. Lines, M. Flynn, J. Large, A. Bostrom, P. Southam, E. J. Keogh, The UEA multivariate time series classification archive, 2018, CoRR abs/1811.00075 (2018).

[72] Y. Su, Y. Zhao, C. Niu, R. Liu, W. Sun, D. Pei, Robust anomaly detection for multivariate time series through stochastic recurrent neural network, in: A. Teredesai, V. Kumar, Y. Li, R. Rosales, E. Terzi, G. Karypis (Eds.), Proceedings of the 25th ACM SIGKDD International Conference on Knowledge Discovery & Data Mining, KDD 2019, Anchorage, AK, USA, August 4-8, 2019, ACM, 2019, pp. 2828–2837.

[73] K. Hundman, V. Constantinou, C. Laporte, I. Colwell, T. Söderström, Detecting spacecraft anomalies

using lstms and nonparametric dynamic thresholding, in: Y. Guo, F. Farooq (Eds.), Proceedings of the 24th ACM SIGKDD International Conference on Knowledge Discovery & Data Mining, KDD 2018, London, UK, August 19-23, 2018, ACM, 2018, pp. 387–395.

[74] A. P. Mathur, N. O. Tippenhauer, Swat: a water treatment testbed for research and training on ICS security, in: 2016 International Workshop on Cyber-physical Systems for Smart Water Networks, CySWater@CPSWeek 2016, Vienna, Austria, April 11, 2016, IEEE Computer Society, 2016, pp. 31–36.

[75] A. Abdulaal, Z. Liu, T. Lancewicki, Practical approach to asynchronous multivariate time series anomaly detection and localization, in: F. Zhu, B. C. Ooi, C. Miao (Eds.), KDD '21: The 27th ACM SIGKDD Conference on Knowledge Discovery and Data Mining, Virtual Event, Singapore, August 14-18, 2021, ACM, 2021, pp. 2485–2494.

[76] J. Xu, H. Wu, J. Wang, M. Long, Anomaly transformer: Time series anomaly detection with association discrepancy, in: The Tenth International Conference on Learning Representations, ICLR 2022, Virtual Event, April 25-29, 2022, OpenReview.net, 2022.

[77] Y. Dong, J. Cordonnier, A. Loukas, Attention is not all you need: pure attention loses rank doubly exponentially with depth, in: M. Meila, T. Zhang (Eds.), Proceedings of the 38th International Conference on Machine Learning, ICML 2021, 18-24 July 2021, Virtual Event, Vol. 139 of Proceedings of Machine Learning Research, PMLR, 2021, pp. 2793–2803.

URL <http://proceedings.mlr.press/v139/dong21a.html>

## Appendix A. Theoretical Proof

### Appendix A.1. Proof of Theorem 1

First, since the heads in the diagonal MHSA layer reach the maximum diagonal pattern measurement value, the attention weights for non-local regions around queries are fixed to 0. There is

$$A_{q,k}^{(h)} = \begin{cases} f^{(q,h)}(q-k) & (q-k) \in \Delta \\ 0 & \text{otherwise} \end{cases}$$

where  $\Delta = \{-\lfloor \lambda/2 \rfloor, \dots, \lfloor \lambda/2 \rfloor\}$  contains all the corresponding shifts in the local region with size  $\lambda$ .  $f^{(q,h)}$  is a set of bijective mappings:  $f^{(q,h)} : \Delta \rightarrow (0, 1)$ . For fixed  $q$  and  $h$ ,  $\sum_{\delta \in \Delta} f^{(q,h)}(\delta) = 1$ . There is:

$$\begin{aligned} MHSA(\mathbf{X})_{q,:}^D &= \sum_{h \in [H]} \sum_{k=1}^N A_{q,k}^{(h)} \mathbf{X}_{k,:} W^{(h)} \\ &= \sum_{h \in [H]} \sum_{\delta \in \Delta} f^{(q,h)}(\delta) \mathbf{X}_{q-\delta,:} W^{(h)} \\ &= \sum_{h \in [H]} \left( \sum_{\delta \in \Delta} \mathbf{X}_{q-\delta,:} W_{\delta}^{(q,h)} \right) \end{aligned}$$

where  $MHSA(\mathbf{X})^D$  is utilized to represent the output of the diagonal MHSA layer, and  $W_{\delta}^{(q,h)} = \text{diag}(f^{(q,h)}(\delta)) W^{(h)}$ . We can observe that the expression inside the parentheses has the same form as the expression for convolution. Therefore,

$$MHSA(\mathbf{X})_{q,:}^D = \sum_{h \in [H]} Conv^h(\mathbf{X})_{q,:}$$

### Appendix A.2. Proof of Theorem 2

For the  $h$ -th head, let  $\tilde{K}^{(h)} = \{\tilde{k}_1^{(h)}, \dots, \tilde{k}_{\lambda}^{(h)}\}$ . For any  $q \in [N]$ , let  $\phi^{(q,h)}$  be a mapping that  $\phi^{(q,h)} : \tilde{K}^{(h)} \rightarrow (0, 1]$ , which satisfies  $\sum_{k \in \tilde{K}^{(h)}} \phi^{(q,h)}(k) = 1$ . The attention score matrix of the  $h$ -th head in a vertical MHSA layer that reaches the maximum vertical pattern measurement value can be denoted as:

$$A_{q,k}^{(h)} = \begin{cases} \phi^{(q,h)}(k) & k \in \tilde{K}^{(h)} \\ 0 & \text{otherwise} \end{cases}$$

Let  $f^{(h)}$  be a mapping that  $f^{(h)} : \tilde{K}^{(h)} \rightarrow \Delta$ , where  $\Delta = \{-\lfloor \lambda/2 \rfloor, \dots, \lfloor \lambda/2 \rfloor\}$ . For any  $q \in [N]$ , let  $\varphi^{(q,h)}$  be a mapping that  $\varphi^{(q,h)} : \Delta \rightarrow (0, 1]$ , which satisfies  $\sum_{\delta \in \Delta} \varphi^{(q,h)}(\delta) = 1$ . Eq.(A.1) can be rewritten as:

$$A_{q,k}^{(h)} = \begin{cases} \varphi^{(q,h)}(q-k) & q-k \in f\left(\tilde{K}^{(h)}\right) = \Delta \\ 0 & \text{otherwise} \end{cases}$$

Thus,

$$\begin{aligned} MHSA(\mathbf{X})_{q,:}^V &= \sum_{h \in [H]} \left( \sum_{k \in [N]} A_{q,k}^{(h)} \mathbf{X}_{k,:} \right) W^{(h)} \\ &= \sum_{h \in [H]} \left( \sum_{\delta \in \Delta} \varphi^{(q,h)}(\delta) \mathbf{X}_{q-\delta,:} \right) W^{(h)} \\ &= \sum_{h \in [H]} \left( \sum_{\delta \in \Delta} \mathbf{X}_{q-\delta,:} W_{\delta}^{(q,h)} \right) \end{aligned}$$

where  $MHSA(\mathbf{X})^V$  is utilized to represent the output of the vertical MHSA layer, and  $W_\delta^{(q,h)} = \text{diag}(\varphi^{(q,h)}(\delta)) W^{(h)}$ . We can observe that the expression inside the parentheses has the same form as the expression for convolution. Therefore,

$$MHSA(\mathbf{X})_{q,:}^V = \sum_{h \in [H]} Conv^h(\mathbf{X})_{q,:}$$

### Appendix A.3. Stationary Analysis

In this section, we will prove that the Surrogate Attention Block is a linear time-invariant system, which can be described by the following equations:

$$\begin{aligned} x_{t+1} &= \mathbf{A}x_t + \mathbf{B}u_{t+1} \\ y_{t+1} &= \mathbf{C}x_{t+1} + \mathbf{D}u_{t+1} \end{aligned}$$

For a time series task,  $x_t$  is the input at time step  $t$ , which is mapped to  $q_t, k_t, v_t$  by linear projection. From Eq.(2), we can derive the output  $y_t$  as:

$$y_t = [m_{t,1}^2 \ m_{t,2}^2 \ \dots \ m_{t,N}^2] \times \left( \begin{bmatrix} k_1 m_{1,1}^1 & k_1 m_{1,2}^1 & \dots & k_1 m_{1,N}^1 \\ k_2 m_{2,1}^1 & k_2 m_{2,2}^1 & \dots & k_2 m_{2,N}^1 \\ \vdots & \vdots & \ddots & \vdots \\ k_N m_{N,1}^1 & k_N m_{N,2}^1 & \dots & k_N m_{N,N}^1 \end{bmatrix} \times \begin{bmatrix} q_1 \\ q_2 \\ \vdots \\ q_N \end{bmatrix} \right) \odot v_t$$

This is clearly a time-varying system, and to relate our approach to time-invariant systems, we treat  $\mathbf{M}_t^2 = [m_{t,1}^2 \ m_{t,2}^2 \ \dots \ m_{t,N}^2]$  as a post-processing step, facilitating the identification of the linear time-invariant components.

By redefining matrices  $\mathbf{A}$ ,  $\mathbf{B}$ ,  $\mathbf{C}$ , and  $\mathbf{D}$ , we observe the system in a new light:

$$\begin{aligned} \mathbf{A} &= 0, \mathbf{B} = \mathbf{I}, \mathbf{D} = 0 \\ \mathbf{C} &= \begin{bmatrix} k_1 m_{1,1}^1 & k_1 m_{1,2}^1 & \dots & k_1 m_{1,N}^1 \\ k_2 m_{2,1}^1 & k_2 m_{2,2}^1 & \dots & k_2 m_{2,N}^1 \\ \vdots & \vdots & \ddots & \vdots \\ k_N m_{N,1}^1 & k_N m_{N,2}^1 & \dots & k_N m_{N,N}^1 \end{bmatrix} \times \begin{bmatrix} q_1 \\ q_2 \\ \vdots \\ q_N \end{bmatrix} \end{aligned}$$

This transformation yields a simplified LTI form:

$$\begin{aligned} x_{t+1} &= \mathbf{B}v_{t+1}, \\ y'_{t+1} &= \mathbf{C}x_{t+1}. \end{aligned}$$

In this context,  $y'_{t+1}$  represents the transformed output without the influence of  $\mathbf{M}_t^2$ , and it serves as a basis for subsequent post-processing. This separation allows for a comprehensive analysis of the LTI properties of the system. We proceed to apply the post-processing step by multiplying  $y'_{t+1}$  with  $\mathbf{M}_t^2$ , facilitating the extraction of temporal features and providing insights into the system's behavior. This decomposition and reformulation underscore the linear time-invariant characteristics of the system, enhancing our understanding of its stability and behavior over time.

#### Appendix A.4. Expressiveness Analysis

Let  $\mathbf{L}^1$ ,  $\mathbf{R}^1$  and  $A$  be as follows:

$$\mathbf{L}^1 = \begin{bmatrix} l_{[0,0]}^1, l_{[0,1]}^1, \dots, l_{[0,\sqrt{N}-1]}^1, \dots \\ l_{[1,0]}^1, l_{[1,1]}^1, \dots, l_{[1,\sqrt{N}-1]}^1, \dots \\ \vdots \\ l_{[\sqrt{N}-1,0]}^1, l_{[\sqrt{N}-1,1]}^1, \dots, l_{[\sqrt{N}-1,\sqrt{N}-1]}^1, \dots \\ \dots, l_{[\sqrt{N},\sqrt{N}]}^1, l_{[\sqrt{N},\sqrt{N}+1]}^1, \dots, l_{[\sqrt{N},2\sqrt{N}-1]}^1, \dots \\ \dots, l_{[\sqrt{N}+1,\sqrt{N}]}^1, l_{[\sqrt{N}+1,\sqrt{N}+1]}^1, \dots, l_{[\sqrt{N}+1,2\sqrt{N}-1]}^1, \dots \\ \vdots \\ \dots, l_{[2\sqrt{N}-1,\sqrt{N}]}^1, l_{[2\sqrt{N}-1,\sqrt{N}+1]}^1, \dots, l_{[2\sqrt{N}-1,2\sqrt{N}-1]}^1, \dots \\ \vdots \\ \dots, l_{[N-1-\sqrt{N},N-1-\sqrt{N}]}^1, l_{[N-1-\sqrt{N},N+\sqrt{N}]}^1, \dots, l_{[N-1-\sqrt{N},N-1]}^1 \\ \dots, l_{[N-\sqrt{N},N-1-\sqrt{N}]}^1, l_{[N-\sqrt{N},N+\sqrt{N}]}^1, \dots, l_{[N-\sqrt{N},N-1]}^1 \\ \vdots \\ \dots, l_{[N-1,N-1-\sqrt{N}]}^1, l_{[N-1,N+\sqrt{N}]}^1, \dots, l_{[N-1,N-1]}^1 \end{bmatrix}$$

$$\mathbf{R}^1 = \begin{bmatrix} r_{[0,0]}^1, r_{[0,1]}^1, \dots, r_{[0,\sqrt{N}-1]}^1, \dots \\ r_{[1,0]}^1, r_{[1,1]}^1, \dots, r_{[1,\sqrt{N}-1]}^1, \dots \\ \vdots \\ r_{[\sqrt{N}-1,0]}^1, r_{[\sqrt{N}-1,1]}^1, \dots, r_{[\sqrt{N}-1,\sqrt{N}-1]}^1, \dots \\ \dots, r_{[\sqrt{N},\sqrt{N}]}^1, r_{[\sqrt{N},\sqrt{N}+1]}^1, \dots, r_{[\sqrt{N},2\sqrt{N}-1]}^1, \dots \\ \dots, r_{[\sqrt{N}+1,\sqrt{N}]}^1, r_{[\sqrt{N}+1,\sqrt{N}+1]}^1, \dots, r_{[\sqrt{N}+1,2\sqrt{N}-1]}^1, \dots \\ \vdots \\ \dots, r_{[2\sqrt{N}-1,\sqrt{N}]}^1, r_{[2\sqrt{N}-1,\sqrt{N}+1]}^1, \dots, r_{[2\sqrt{N}-1,2\sqrt{N}-1]}^1, \dots \\ \vdots \\ \dots, r_{[N-1-\sqrt{N},N-1-\sqrt{N}]}^1, r_{[N-1-\sqrt{N},N+\sqrt{N}]}^1, \dots, r_{[N-1-\sqrt{N},N-1]}^1 \\ \dots, r_{[N-\sqrt{N},N-1-\sqrt{N}]}^1, r_{[N-\sqrt{N},N+\sqrt{N}]}^1, \dots, r_{[N-\sqrt{N},N-1]}^1 \\ \vdots \\ \dots, r_{[N-1,N-1-\sqrt{N}]}^1, r_{[N-1,N+\sqrt{N}]}^1, \dots, r_{[N-1,N-1]}^1 \end{bmatrix}$$

$$A = \mathbf{M}^1 Q \odot K = \begin{bmatrix} a_0 \\ a_1 \\ \vdots \\ a_{N-1} \end{bmatrix}$$

where  $\mathbf{R}^1$  and  $\mathbf{L}^1$  are block diagonal matrices of size  $N \times N$ , with each block having dimensions  $\sqrt{N} \times \sqrt{N}$ . Let  $b$  and  $c$  represent the abscissa and ordinate of the elements in the

diagonal blocks of  $\mathbf{R}^1$  and  $\mathbf{L}^1$ . If  $\lfloor b/\sqrt{N} \rfloor \neq \lfloor c/\sqrt{N} \rfloor$ , then  $\mathbf{R}_{[b,c]}^1 = \mathbf{L}_{[b,c]}^1 = 0$ .

It is important to note that the superscript in the upper right corner of the matrix or element denotes its identification, while the subscript in the lower right corner indicates the element's index within the matrix. For example,  $m_{[0,0]}^2$  signifies the element located at coordinates  $[0, 0]$  within  $\mathbf{M}^2$ , rather than the square of  $m_{[0,0]}$ .

Given the following matrix definitions:

$$\mathbf{M}^1 = P\mathbf{L}^1P\mathbf{R}^1P, \mathbf{M}^2 = P\mathbf{L}^2P\mathbf{R}^2P$$

where  $P$  is a permutation matrix. Let  $h(i) = \lfloor i/\sqrt{N} \rfloor + \sqrt{N}(i\% \sqrt{N})$ , The subsequent calculation process follows this redefinition, illustrating the transformation of these matrices based on these block structures. The detailed process is as follows:

$$P\mathbf{L}^1 = \begin{bmatrix} l_{[0,0]}^1, l_{[0,1]}^1, \dots, l_{[0,\sqrt{N}-1]}^1, \dots \\ l_{[\sqrt{N},0]}^1, l_{[\sqrt{N},1]}^1, \dots, l_{[\sqrt{N},\sqrt{N}-1]}^1, \dots \\ \vdots \\ l_{[\sqrt{N}(\sqrt{N}-1),0]}^1, l_{[\sqrt{N}(\sqrt{N}-1),1]}^1, \dots, l_{[\sqrt{N}(\sqrt{N}-1),\sqrt{N}-1]}^1, \dots \\ \dots, l_{[1,\sqrt{N}]}^1, l_{[1,\sqrt{N}+1]}^1, \dots, l_{[1,2\sqrt{N}-1]}^1, \dots \\ \dots, l_{[1+\sqrt{N},\sqrt{N}]}^1, l_{[1+\sqrt{N},\sqrt{N}+1]}^1, \dots, l_{[1+\sqrt{N},2\sqrt{N}-1]}^1, \dots \\ \vdots \\ \dots, l_{[1+\sqrt{N}(\sqrt{N}-1),\sqrt{N}]}^1, l_{[1+\sqrt{N}(\sqrt{N}-1),\sqrt{N}+1]}^1, \dots, l_{[1+\sqrt{N}(\sqrt{N}-1),2\sqrt{N}-1]}^1, \dots \\ \vdots \\ \dots, l_{[\sqrt{N}-1,N-1-\sqrt{N}]}^1, l_{[\sqrt{N}-1,N+\sqrt{N}]}^1, \dots, l_{[\sqrt{N}-1,N-1]}^1 \\ \dots, l_{[2\sqrt{N}-1,N-1-\sqrt{N}]}^1, l_{[2\sqrt{N}-1,N+\sqrt{N}]}^1, \dots, l_{[2\sqrt{N}-1,N-1]}^1 \\ \vdots \\ \dots, l_{[N-1,N-1-\sqrt{N}]}^1, l_{[N-1,N+\sqrt{N}]}^1, \dots, l_{[N-1,N-1]}^1 \end{bmatrix}$$

$$P\mathbf{L}^1P = \begin{bmatrix} l_{[0,0]}^1, l_{[0,\sqrt{N}]}^1, \dots, l_{[0,\sqrt{N}(\sqrt{N}-1)]}^1, \dots \\ l_{[\sqrt{N},0]}^1, l_{[\sqrt{N},\sqrt{N}]}^1, \dots, l_{[\sqrt{N},\sqrt{N}(\sqrt{N}-1)]}^1, \dots \\ \vdots \\ l_{[\sqrt{N}(\sqrt{N}-1),0]}^1, l_{[\sqrt{N}(\sqrt{N}-1),\sqrt{N}]}^1, \dots, l_{[\sqrt{N}(\sqrt{N}-1),\sqrt{N}(\sqrt{N}-1)]}^1, \dots \\ \dots, l_{[1,1]}^1, l_{[1,1+\sqrt{N}]}^1, \dots, l_{[1,1+\sqrt{N}(\sqrt{N}-1)]}^1, \dots \\ \dots, l_{[1+\sqrt{N},1]}^1, l_{[1+\sqrt{N},1+\sqrt{N}]}^1, \dots, l_{[1+\sqrt{N},1+\sqrt{N}(\sqrt{N}-1)]}^1, \dots \\ \vdots \\ \dots, l_{[1+\sqrt{N}(\sqrt{N}-1),1]}^1, l_{[1+\sqrt{N}(\sqrt{N}-1),1+\sqrt{N}]}^1, \dots, l_{[1+\sqrt{N}(\sqrt{N}-1),1+\sqrt{N}(\sqrt{N}-1)]}^1, \dots \\ \vdots \\ \dots, l_{[\sqrt{N}-1,\sqrt{N}-1]}^1, l_{[\sqrt{N}-1,2\sqrt{N}-1]}^1, \dots, l_{[\sqrt{N}-1,N-1]}^1 \\ \dots, l_{[2\sqrt{N}-1,\sqrt{N}-1]}^1, l_{[2\sqrt{N}-1,2\sqrt{N}-1]}^1, \dots, l_{[2\sqrt{N}-1,N-1]}^1 \\ \vdots \\ \dots, l_{[N-1,\sqrt{N}-1]}^1, l_{[N-1,2\sqrt{N}-1]}^1, \dots, l_{[N-1,N-1]}^1 \end{bmatrix}$$

$$P\mathbf{L}^1P\mathbf{R}^1 = \begin{bmatrix} \sum_{i=0}^{N-1} l_{[0,h(i)]}^1 r_{[i,0]}^1, \sum_{i=0}^{N-1} l_{[0,h(i)]}^1 r_{[i,1]}^1, \dots \\ \sum_{i=0}^{N-1} l_{[\sqrt{N},h(i)]}^1 r_{[i,0]}^1, \sum_{i=0}^{N-1} l_{[\sqrt{N},h(i)]}^1 r_{[i,1]}^1, \dots \\ \vdots \\ \sum_{i=0}^{N-1} l_{[\sqrt{N}(\sqrt{N}-1),h(i)]}^1 r_{[i,0]}^1, \sum_{i=0}^{N-1} l_{[\sqrt{N}(\sqrt{N}-1),h(i)]}^1 r_{[i,1]}^1, \dots \\ \vdots \end{bmatrix}$$

$$\mathbf{M}^1 = P\mathbf{L}^1P\mathbf{R}^1P = \begin{bmatrix} \sum_{i=0}^{N-1} l_{[0,h(i)]}^1 r_{[i,0]}^1, \sum_{i=0}^{N-1} l_{[0,h(i)]}^1 r_{[i,\sqrt{N}]}^1, \dots \\ \sum_{i=0}^{N-1} l_{[\sqrt{N},h(i)]}^1 r_{[i,0]}^1, \sum_{i=0}^{N-1} l_{[\sqrt{N},h(i)]}^1 r_{[i,\sqrt{N}]}^1, \dots \\ \vdots \\ \sum_{i=0}^{N-1} l_{[\sqrt{N}(\sqrt{N}-1),h(i)]}^1 r_{[i,0]}^1, \sum_{i=0}^{N-1} l_{[\sqrt{N}(\sqrt{N}-1),h(i)]}^1 r_{[i,\sqrt{N}]}^1, \dots \\ \vdots \end{bmatrix}$$

$\mathbf{M}^2$  can be obtained in the same way:

$$\mathbf{M}^2 = \begin{bmatrix} \sum_{i=0}^{N-1} l_{[0,h(i)]}^2 r_{[i,0]}^2, \sum_{i=0}^{N-1} l_{[0,h(i)]}^2 r_{[i,\sqrt{N}]}^2, \dots \\ \sum_{i=0}^{N-1} l_{[\sqrt{N},h(i)]}^2 r_{[i,0]}^2, \sum_{i=0}^{N-1} l_{[\sqrt{N},h(i)]}^2 r_{[i,\sqrt{N}]}^2, \dots \\ \vdots \\ \sum_{i=0}^{N-1} l_{[\sqrt{N}(\sqrt{N}-1),h(i)]}^2 r_{[i,0]}^2, \sum_{i=0}^{N-1} l_{[\sqrt{N}(\sqrt{N}-1),h(i)]}^2 r_{[i,\sqrt{N}]}^2, \dots \\ \vdots \end{bmatrix} = \begin{bmatrix} m_{[0,0]}^2, m_{[0,1]}^2, \dots \\ m_{[1,0]}^2, m_{[1,1]}^2, \dots \\ \vdots \\ m_{[\sqrt{N}-1,0]}^2, m_{[\sqrt{N}-1,1]}^2, \dots \\ \vdots \end{bmatrix}$$

$$\begin{aligned}
\mathbf{M}^1 Q \odot K &= \begin{bmatrix} (\sum_{i=0}^{N-1} l_{[0,h(i)]}^1 r_{[i,0]}^1 q_0 + \sum_{i=0}^{N-1} l_{[0,h(i)]}^1 r_{[i,\sqrt{N}]}^1 q_1 + \dots) k_0 \\ (\sum_{i=0}^{N-1} l_{[\sqrt{N},h(i)]}^1 r_{[i,0]}^1 q_0 + \sum_{i=0}^{N-1} l_{[\sqrt{N},h(i)]}^1 r_{[i,\sqrt{N}]}^1 q_1 + \dots) k_1 \\ \vdots \\ (\sum_{i=0}^{N-1} l_{[\sqrt{N}(\sqrt{N}-1),h(i)]}^1 r_{[i,0]}^1 q_0 + \sum_{i=0}^{N-1} l_{[\sqrt{N}(\sqrt{N}-1),h(i)]}^1 r_{[i,\sqrt{N}]}^1 q_1 + \dots) k_{\sqrt{N}-1} \\ \vdots \end{bmatrix} \\
\mathbf{M}^2(\mathbf{M}^1 Q \odot K) &= \mathbf{M}^2 A = \begin{bmatrix} \sum_{i=0}^{N-1} m_{[0,i]}^2 a_i \\ \sum_{i=0}^{N-1} m_{[1,i]}^2 a_i \\ \vdots \\ \sum_{i=0}^{N-1} m_{[\sqrt{N}-1,i]}^2 a_i \\ \vdots \end{bmatrix} \\
\mathbf{Y} = \mathbf{M}^2(\mathbf{M}^1 Q \odot K) \odot V &= \begin{bmatrix} \sum_{j=0}^{N-1} m_{[0,j]}^2 a_j v_0 \\ \sum_{j=0}^{N-1} m_{[1,j]}^2 a_j v_1 \\ \vdots \\ \sum_{j=0}^{N-1} m_{[\sqrt{N}-1,j]}^2 a_j v_{\sqrt{N}-1} \\ \vdots \end{bmatrix} = \begin{bmatrix} y_0 \\ y_1 \\ \vdots \\ y_{\sqrt{N}-1} \\ \vdots \end{bmatrix}
\end{aligned}$$

So we can get

$$\begin{aligned}
y_k &= \sum_{j=0}^{N-1} m_{[k,j]}^2 a_j v_k = v_k (m_{[k,0]}^2 a_0 + \dots + m_{[k,k-1]}^2 a_{k-1} + \dots) \\
&= v_k \{ [(\sum_{i=0}^{N-1} l_{[h(k),h(i)]}^2 r_{[i,0]}^2) (\sum_{i=0}^{N-1} l_{[0,h(i)]}^1 r_{[i,0]}^1 q_0 + \dots) k_0] + \dots \\
&\quad + [(\sum_{i=0}^{N-1} l_{[h(k),h(i)]}^2 r_{[i,h(k-1)]}^2) (\sum_{i=0}^{N-1} l_{[h(k-1),h(i)]}^1 r_{[i,0]}^1 q_0 + \dots + \sum_{i=0}^{N-1} l_{[h(k-1),h(i)]}^1 r_{[i,h(k-1)]}^1 q_{k-1} + \dots) k_{k-1}] + \dots \}
\end{aligned}$$

To evaluate the behavior of the Surrogate Attention Block in terms of capturing long-term and short-term dependencies, we can ignore the projections of queries, keys, and values for simplicity.

Let's consider a case where specific elements within matrices are set to 1, while others are set to 0, allowing us to isolate specific correlations. Define these conditions for the Surrogate Attention Block:

1. *Long-Term Dependencies:* Let  $l_{[h(k),h(i)]}^2 = r_{[i,0]}^2 = l_{[0,h(i)]}^1 = r_{[i,0]}^1 = 1$ , with all other elements set to 0. Under these conditions, if we calculate:

$$\sum_{i=0}^{N-1} l_{[h(k),h(i)]}^2 r_{[i,h(k-1)]}^2 = \sum_{i=0}^{N-1} l_{[0,h(i)]}^1 r_{[i,0]}^1 = 1$$

It yields that the output at time step  $k$ , denoted by  $y_k$ , is equivalent to  $x_k x_0^2$ . This indicates that the attention mechanism strongly correlates time step  $k$  with time step 0, thereby validating that the Surrogate Attention Block can effectively capture long-term dependencies.

2. *Short-Term Dependencies*: Similarly, let  $l_{[h(k), h(i)]}^2 = r_{[i, h(k-1)]}^2 = l_{[h(k-1), h(i)]}^1 = r_{[i, h(k-1)]}^1 = 1$ , with other elements set to 0. If we calculate:

$$\sum_{i=0}^{N-1} l_{[h(k), h(i)]}^2 r_{[i, h(k-1)]}^2 = \sum_{i=0}^{N-1} l_{[h(k-1), h(i)]}^1 r_{[i, h(k-1)]}^1 = 1$$

It leads to the result that  $y_k = x_k x_{k-1}^2$ . This configuration confirms that the attention mechanism creates a strong correlation between time step  $k$  and time step  $k-1$ , suggesting that the Surrogate Attention Block is also capable of learning short-term dependencies.

## Appendix B. Experiment details

### Appendix B.1. Metrics

- **MAE (Mean Absolute Error)** measures the average absolute difference between the actual values and predicted values. It provides a straightforward and interpretable measure of prediction accuracy. A lower MAE indicates that the model tends to make predictions that are closer to the actual values in magnitude. Formula:

$$MAE = \frac{1}{n} \sum_{i=1}^n |y_i - \hat{y}_i|$$

- **MSE (Mean Squared Error)** calculates the average of the squared differences between actual and predicted values. MSE is sensitive to large errors and penalizes them more than MAE. It is commonly used for its mathematical tractability and suitability for optimization algorithms. Formula:

$$MSE = \frac{1}{n} \sum_{i=1}^n (y_i - \hat{y}_i)^2$$

- **R-Square (Coefficient of Determination)** evaluates the goodness of fit of a model to the data. It quantifies the proportion of the variance in the dependent variable that is explained by the model. R-Square values range from 0 to 1, with higher values indicating that the model captures a larger portion of the variation in the data. It helps assess how well the model represents the underlying data patterns. Formula:

$$R^2 = 1 - \frac{\sum_{i=1}^n (y_i - \hat{y}_i)^2}{\sum_{i=1}^n (y_i - \bar{y})^2}$$

- **DTW (Dynamic Time Wrapping)** is a method used for comparing two time series with potentially different lengths and time axes. It determines the optimal alignment of elements in the two series, minimizing their paired distances. Therefore, DTW can be used for measuring the waveform similarity between two time series. DTW calculates the alignment between two time series by finding the optimal path through a cost matrix. The optimal path  $P$  is determined by minimizing the accumulated cost:

$$DTW = \min_P \sqrt{\sum_{(i,j) \in P} |y_i - \hat{y}_i|}$$

- **SMAPE (Symmetric Mean Absolute Percentage Error)** is a symmetric percentage-based error metric widely used in short-term time series forecasting. It measures the percentage difference between the actual and predicted values, accommodating situations where the scale of the data varies. Formula:

$$SMAPE = \frac{1}{n} \sum_{i=1}^n \frac{|y_i - \hat{y}_i|}{(|y_i| + |\hat{y}_i|)/2} \times 100$$

- **MASE (Mean Absolute Scaled Error)** is a scale-independent metric that evaluates the accuracy of a forecasting model. It compares the mean absolute error of the model to the mean absolute error of a naïve forecast, providing a standardized measure of performance. Formula:

$$MASE = \frac{1}{n} \sum_{i=1}^n \frac{|y_i - \hat{y}_i|}{\frac{1}{n-1} \sum_{i=2}^n |y_i - y_{i-1}|}$$

- **OWA (Overall Weighted Average)** is a special metric used in M4 competition. Formula:

$$OWA = \frac{1}{2} \left( \frac{SMAPE}{SMAPE_{Naive}} + \frac{MASE}{MASE_{Naive}} \right)$$

- **Accuracy** is a classification metric that measures the proportion of correct predictions out of the total predictions made by a model. Formula:

$$Accuracy = \frac{\text{Number of Correct Predictions}}{\text{Total Number of Predictions}}$$

- **Precision** assesses the accuracy of positive predictions. It is the ratio of true positive predictions to the total number of positive predictions made by the model. Formula:

$$Precision = \frac{\text{True Positives}}{\text{True Positives} + \text{False Positives}}$$

- **Recall (Sensitivity or True Positive Rate)** measures the ability of a model to identify all relevant instances. It is the ratio of true positive predictions to the total number of actual positive instances. Formula:

$$Recall = \frac{\text{True Positives}}{\text{True Positives} + \text{False Negatives}}$$

- **F1-Score** is the harmonic mean of precision and recall. It provides a balance between precision and recall, making it suitable for situations where there is an uneven class distribution. Formula:

$$F1 - Score = 2 \times \frac{\text{Precision} \times \text{Recall}}{\text{Precision} + \text{Recall}}$$

## Appendix B.2. Model Details

This section will show the details of all 9 models of *X-formers* improved with structured matrices. **Bold** indicates sections that have been replaced.

Encoder:			N
Inputs	1 × 3 Conv1d	Embedding(d = 512)	
	<b>Surrogate Attention Block</b> (h = 8, d = 64)		
	Add, LayerNorm, Dropout (p = 0.05)		
Self-attention Block	<b>Surrogate FFN Block</b> , GELU		2
	Add, LayerNorm, Dropout (p = 0.05)		
Decoder:			N
Inputs	1 × 3 Conv1d	Embedding(d = 512)	
Masked PSB	add Mask on Attention Block		
	<b>Surrogate Attention Block</b> (h = 8, d = 64)		
	Add, LayerNorm, Dropout (p = 0.05)		
Self-attention Block	MultiHeadedAttention (h = 8, d = 64)		1
	Add, LayerNorm, Dropout (p = 0.05)		
	<b>Surrogate FFN Block</b> , GELU		
	Add, LayerNorm, Dropout (p = 0.05)		
Final:			
Outputs		FCN	

Table B.16: Details of the improved Vanilla Transformer with structured matrices.

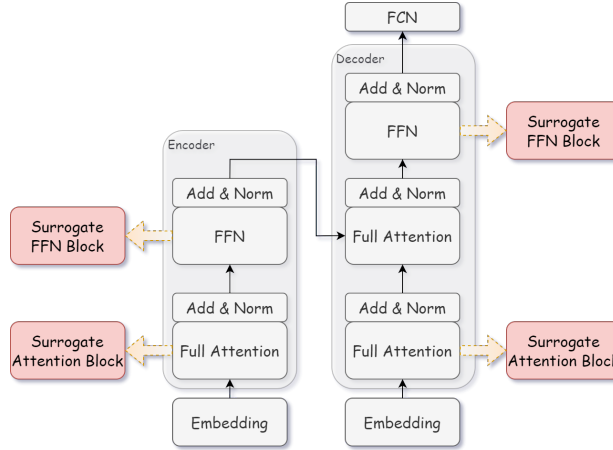


Figure B.11: Architecture of the improved Vanilla Transformer with structured matrices. The red blocks represent the replaced blocks.

Encoder:				N
Inputs	1 × 3 Conv1d	Embedding(d = 512)		
	Surrogate Attention Block (h = 8, d = 64)			
	Add, LayerNorm, Dropout (p = 0.05)			
ProbSparse Self-attention Block	Surrogate FFN Block, GELU			
	Add, LayerNorm, Dropout (p = 0.05)			2
	Series decomposition (moving avg = 25)			
	1 × 3 Conv1d, GELU			
Distilling	Max pooling (stride = 2)			
Decoder:				N
Inputs	1 × 3 Conv1d	Embedding(d = 512)		
Masked PSB	add Mask on Attention Block			
	Surrogate Attention Block (h = 8, d = 64)			
	Add, LayerNorm, Dropout (p = 0.05)			
ProbSparse Self-attention Block	Multi-head ProbSparse Attention (h = 8, d = 64)			1
	Add, LayerNorm, Dropout (p = 0.05)			
	Surrogate FFN Block, GELU			
	Add, LayerNorm, Dropout (p = 0.05)			
Final:				
Outputs		FCN		

Table B.17: Details of the improved Informer with structured matrices.

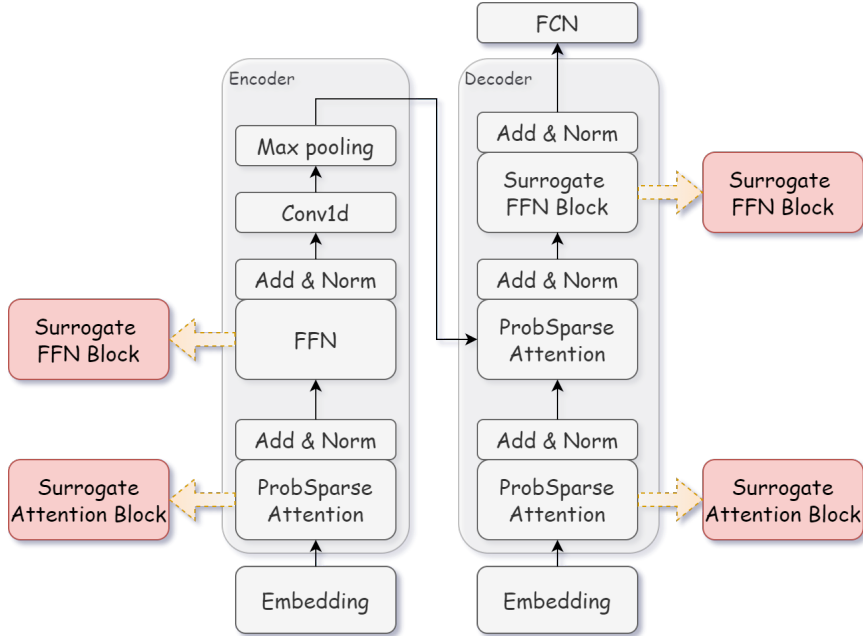


Figure B.12: Architecture of the improved Informer with structured matrices. The red blocks represent the replaced blocks.

Encoder:			N
Inputs	1 × 3 Conv1d	Embedding(d = 512)	
Auto-Correlation Block	<b>Surrogate Attention Block</b> (h = 8, d = 64)		
	Add, Dropout (p = 0.05)		
	Series decomposition (moving avg = 25)		
	<b>Surrogate FFN Block</b> , GELU		2
	Add, Dropout (p = 0.05)		
	Series decomposition (moving avg = 25)		
Decoder:			N
Masked Auto-Correlation Block	Series decomposition (moving avg = 25)		
	1 × 3 Conv1d	Embedding(d = 512)	
	add Mask on Auto-Correlation Block		
	<b>Surrogate Attention Block</b> (h = 8, d = 64)		
	Add, Dropout (p = 0.05)		
	Series decomposition (moving avg = 25)		
	Auto-Correlation (h = 8, d = 64)		
	Add, Dropout (p = 0.05)		1
	Series decomposition (moving avg = 25)		
	<b>Surrogate FFN Block</b> , GELU		
Auto-Correlation Block	Add, Dropout (p = 0.05)		
	Series decomposition (moving avg = 25)		
Final:			
Outputs		FCN	

Table B.18: Details of the improved Autoformer with structured matrices.

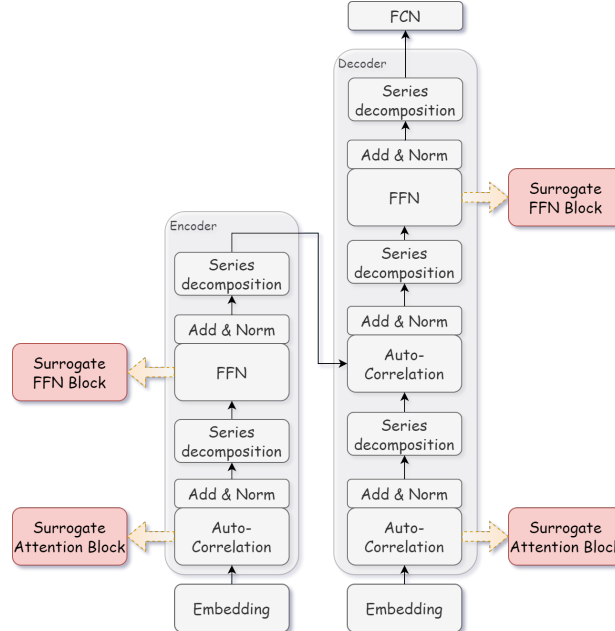


Figure B.13: Architecture of the improved Autoformer with structured matrices. The red blocks represent the replaced blocks.

<b>Encoder:</b>		N
Inputs	Series_decomp(kernel_size=24)	
	TokenEmbedding(d_model=512)	
	TemporalEmbedding(d_model=512)	
Frequency Enhanced Block	Surrogate Attention Block (h = 8, d = 64)	
	Add, Dropout (p = 0.05)	
	Series_decomp(kernel_size=24)	
	Surrogate FFN Block	2
	Add, Dropout (p = 0.05)	
	Series_decomp (kernel_size=24)	
<b>Decoder:</b>		N
Inputs	Series_decomp(kernel_size=24)	
	TokenEmbedding(d_model=512)	
	TemporalEmbedding(d_model=512)	
	The output of Encoder	
Frequency Enhanced Block	Surrogate Attention Block (h = 8, d = 64)	
	Add, Dropout (p = 0.05)	
	Series.decomp (kernel.size=24)	
	Projection (d = 512)	
	MultiWaveletCross/ FourierCrossAttention (h = 8, d = 64)	
	Projection (d = 512)	1
Frequency Enhanced Attention	Add, Dropout (p = 0.05)	
	Series.decomp (kernel.size=24)	
	Surrogate FFN Block	
	Add, Dropout (p = 0.05)	
	Series.decomp (kernel.size=24)	
<b>Final:</b>		
Outputs	FCN	

Table B.19: Details of the improved FEDformer with structured matrices.

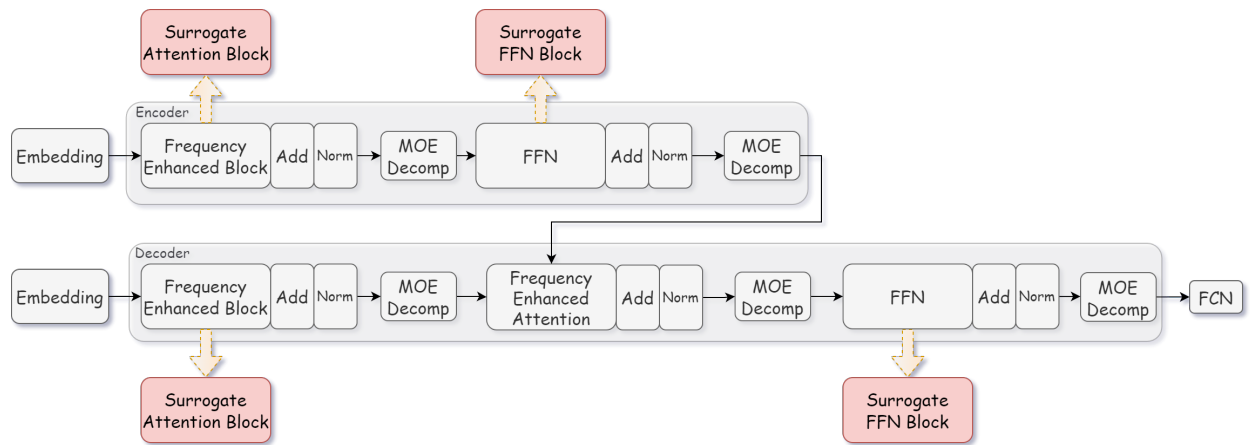


Figure B.14: Architecture of the improved FEDformer with structured matrices. The red blocks represent the replaced blocks.

Encoder:		N
Inputs	DSW_embedding(seg_len=6, d_model=256) LayerNorm(d_model=256)	
Scale Block	SegMerging(d_model=265, win_size=2, nn.LayerNorm) TwoStageAttentionLayer(seg_num=6, factor=10, d_model=256, n_heads=4, d_ff=512, dropout=0.2)	3
Decoder:		N
Inputs	The output of Encoder , The position of embedding	
	<b>Surrogate Attention Block</b> (d_model=256, n_heads=4, dropout = 0.2)	
	Add,Dropout(p=0.2) LayerNorm(d =256)	
	AttentionLayer(d_model=256, n_heads=4, dropout = 0.2)	
TwoStageAttentionLayer	AttentionLayer(d_model=256, n_heads=4, dropout = 0.2) Add,Dropout(p=0.2),LayerNorm(d =256) <b>Surrogate FFN Block</b> , GELU Add,Dropout(p=0.2),LayerNorm(d =256)	4
	AttentionLayer(d_model=256, n_heads=4, dropout = 0.2) Dropout(p=0.2) LayerNorm(d_mode=256) <b>Surrogate FFN Block</b> , GELU LayerNorm(d_model=256) Linear(d_model=256, seg_len=6)	
Final:		
Outputs	FCN	

Table B.20: Details of the improved Crossformer with structured matrices.

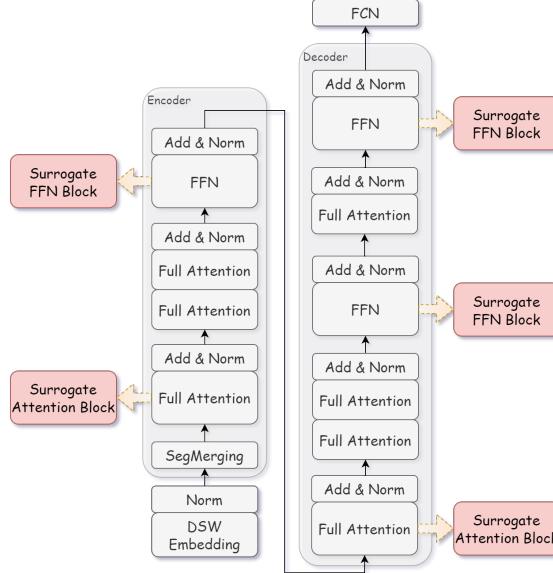


Figure B.15: Architecture of the improved Crossformer with structured matrices. The **red blocks** represent the replaced blocks.

Encoder:		N
Inputs	Embedding(d=512)	
	Mask(input_size=168/169, window_size= '[4, 4, 4]', inner_size=3)	
	Bottleneck_Construct(d_model=512, d_inner=512, window_size= '[4, 4, 4]')	
Attention	<b>Surrogate Attention Block</b> (n_head=4, d_model=512,d)	
	LayerNorm(d_in=512, eps=1e-6)	
PositionwiseFeedForward	<b>Surrogate FFN Block</b> , GELU	
	LayerNorm(d_in=512, eps=1e-6)	
Decoder:		N
Inputs	Embedding(d=512)	
	Mask(input_size=168/169, window_size= '[4, 4, 4]', inner_size=3)	
Attention	<b>Surrogate Attention Block</b> (n_head=4, d_model=512)	
	LayerNorm(d_in=512, eps=1e-6)	
PositionwiseFeedForward	<b>Surrogate FFN Block</b> , GELU	2
	LayerNorm(d_in=512, eps=1e-6)	
Final:		
Outputs	Linear(dim=512/2048)	

Table B.21: Details of the improved Pyraformer with structured matrices.

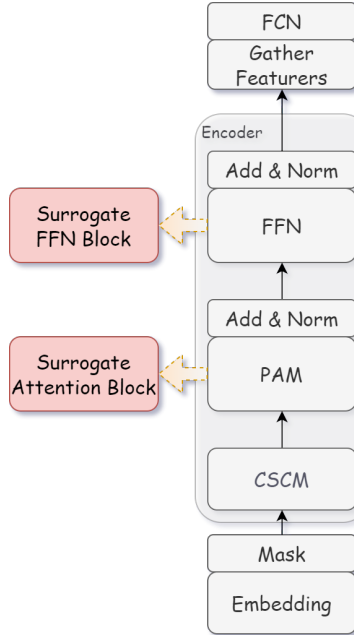


Figure B.16: Architecture of the improved Pyraformer with structured matrices. The red blocks represent the replaced blocks.

Encoder:			N
Inputs		Normalization (dim = 0)	
		Embedding(d = 512)	
		Surrogate Attention Block (h = 8, d = 64)	
		Add & Norm	2
		Surrogate FFN Block, GELU	
		Add & Norm	
Decoder:			N
Inputs	ConCat	Embedding(d = 512)	
		Surrogate Attention Block (h = 8, d = 64)	
		Add & Norm	
		De-stationary Attention ( $\tau, \Delta = 0$ )	
		Add & Norm	1
		Surrogate FFN Block, GELU	
		Add & Norm	
Final:			
Outputs		De-normalizltion ( $\mu_x, \sigma_x$ )	

Table B.22: Details of the improved Non-stationary Transformers with structured matrices.

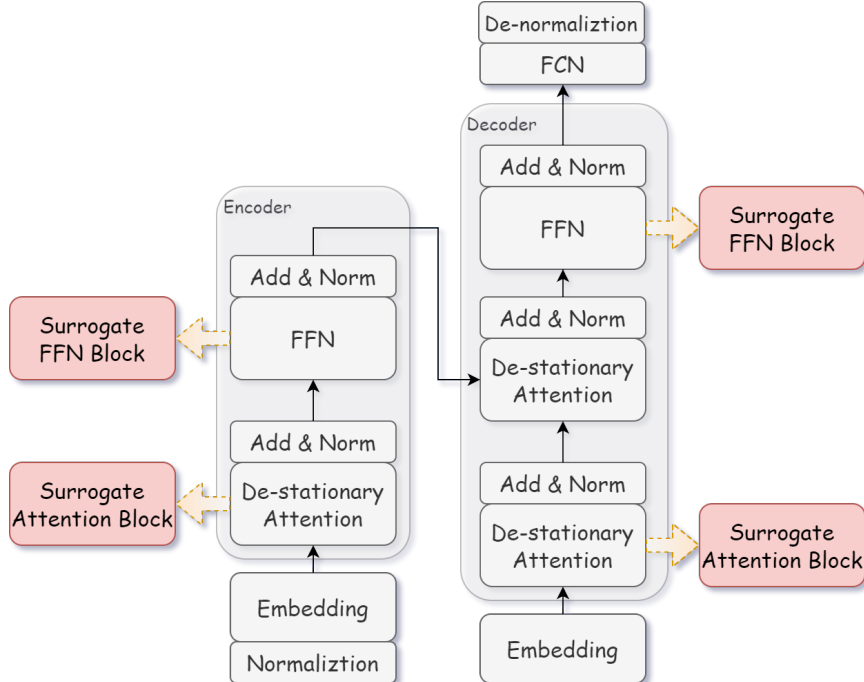


Figure B.17: Architecture of the improved Non-stationary Transformers with structured matrices. The red blocks represent the replaced blocks.

<b>Encoder:</b>		N
	Inputs	
	Normalization (dim = 0)	
	Patching (patch_len=16, stride=8)	
	Embedding (d = 512)	
	<b>Surrogate Attention Block</b> (h = 8, d = 64)	
	Add & Norm	2
	<b>Surrogate FFN Block</b>	
	Add & Norm	
	Reshape (n = Number of variables)	
<b>Decoder:</b>		N
	Flatten (start_dim=-2)	
	Linear Projection (d = pred_len)	1
	Dropout (p = 0.05)	
<b>Final:</b>		
Outputs	De-normalization ( $\mu_x, \sigma_x$ )	

Table B.23: Details of the improved PatchTST with structured matrices.

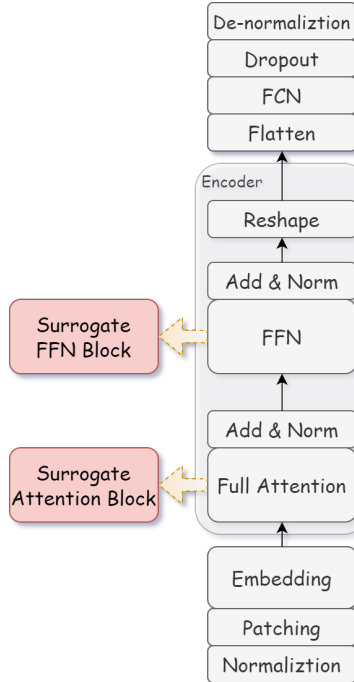


Figure B.18: Architecture of the improved PatchTST with structured matrices. The red blocks represent the replaced blocks.

Encoder:		N
Inputs	Normalizltion (dim = 0)	
	Inverse	
	Embedding(d = 512)	
	<b>Surrogate Attention Block</b> (h = 8, d = 64)	2
	Add & Norm	
	<b>Surrogate FFN Block</b>	
	Add & Norm	
Decoder:		N
	Linear Projection (d = pred_len)	1
Final:		
Outputs	De-normalizltion ( $\mu_x, \sigma_x$ )	

Table B.24: Details of the improved iTransformer with structured matrices.

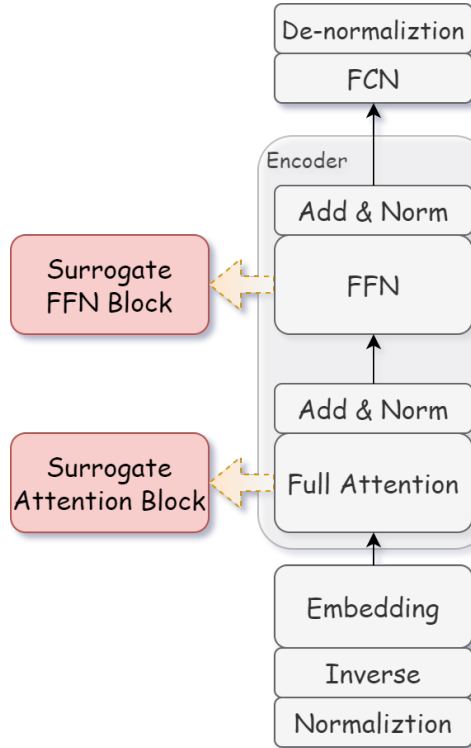


Figure B.19: Architecture of the improved iTransformer with structured matrices. The red blocks represent the replaced blocks.